Source	Geometry	References for Effect
μ^+ depth	Fig. 15, Sec. 4.1.5	Sec. 6.1.1, E.2.1
Back plate	Fig. 8	Fig. 27, Sec. 5.10, 6.6, E.2.2
$T1$	Fig. 15, Sec. 4.1.5	Fig. 17-20, Sec. 5.1, 6.1.2, E.2.3
Detector ineff.	Fig. 8, 11, Sec. 4.1.8	Fig. 21, Sec. 5.2, 6.1.6, E.2.4
μ^+ spin angle		Sec. A.2, E.2.5
Cables	Fig. 8	Fig. 22, Sec. 5.3, 6.1.5, E.2.6
$K2$	Fig. 8, Sec. 4.1.6	Fig. 23, Sec. 5.5, 6.1.4, E.2.7
$C1$	Fig. 8, Sec. 4.1.6	Fig. 25, Sec. 5.9, 6.1.4, E.2.8
P_{max} calib.	Sec. 4.1.1	Sec. 6.4, B.4, E.2.9, 4.1.2
Beam centering		Sec. A.1, E.2.10
Muon stops	Fig. 15, 16	Sec. 6.5, E.2.11
$K3$	Fig. 8, Sec. 4.1.6	Fig. 24, Sec. 5.6, 6.1.4, E.2.12
Line shape	Fig. 13, 14, 30	Sec. E.2.13
$C2$	Fig. 8, Sec. 4.1.6	Fig. 26, Sec. 5.9, 6.1.4, E.2.14
Asymmetry		Sec. A.3, E.2.15
Miscellaneous	Fig. 8	Sec. 5.4, 5.7, 6.1.4, E.2.16

Table 6.2: References to information on the systematic errors.

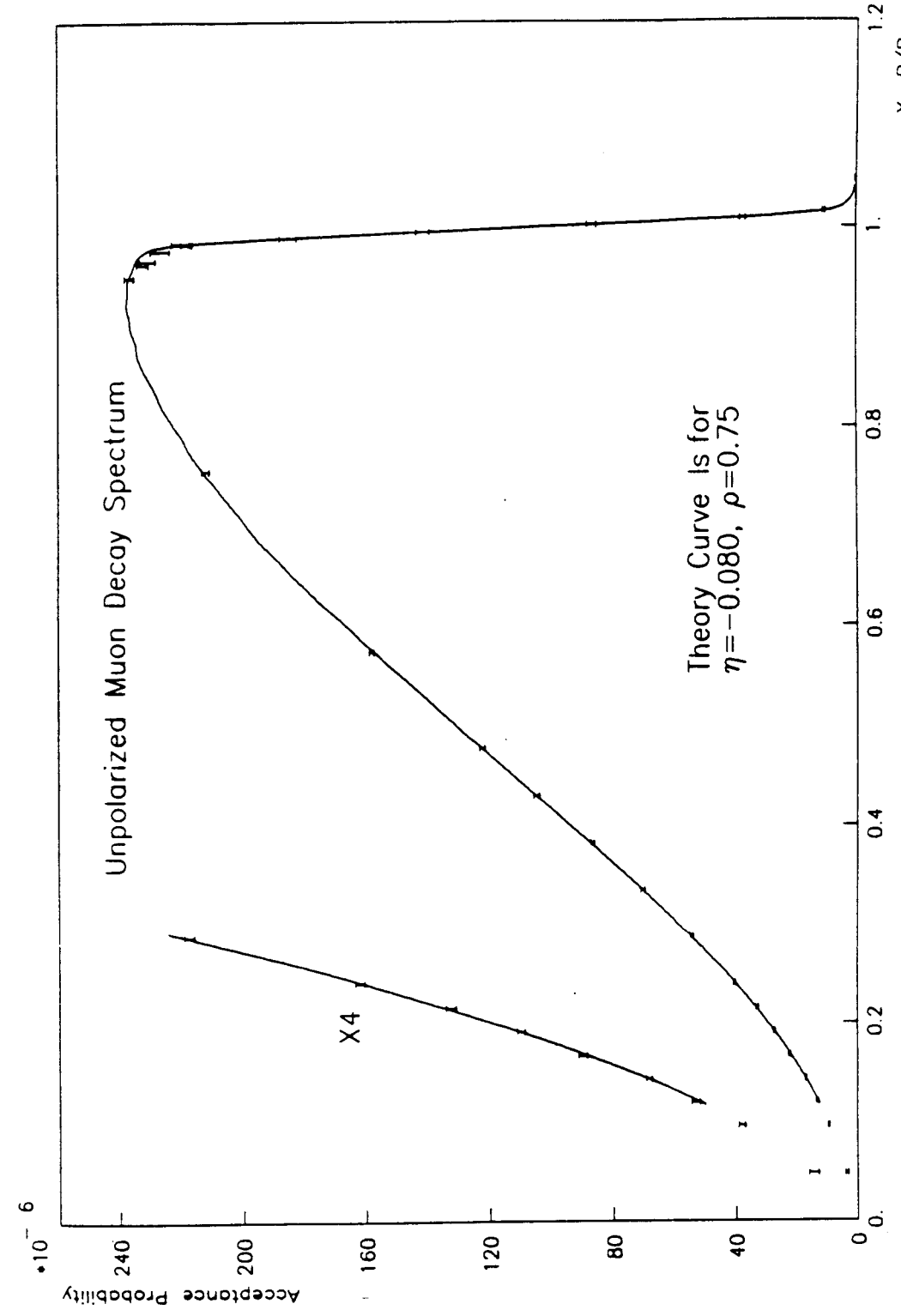

Figure 30. Data points imposed on the corrected theory spectrum for $\rho = 3/4$, and the best-fit values of η and amplitude normalization. Error bars represent only the statistical errors of the data.

- The incoming beam pipe is surrounded by magnetic shielding near the target which might, in principle, distort the field there.
- The earth's field is certainly not along the spectrometer axis and, at low P_{tune} would cause a significant problem if the flux lines were not adequately shunted away by the nearby iron.

A second system of coordinates $\hat{x}'$,$\hat{y}'$,$\hat{z}'$ and angles θ_B,ϕ_B are now defined. The direction of $\hat{z}'$ is defined to be along $\vec{B}$ at the muon position, separated from $\hat{z}$ by the angle θ_B. The coordinate transformation is given by

$$\begin{aligned}
\hat{x}' &= \hat{x}\cos\theta_B\cos\phi_B + \hat{y}\cos\theta_B\sin\phi_B - \hat{z}\sin\theta_B \\
\hat{y}' &= -\hat{x}\sin\phi_B + \hat{y}\cos\phi_B \\
\hat{z}' &= \hat{x}\sin\theta_B\cos\phi_B + \hat{y}\sin\theta_B\sin\phi_B + \hat{z}\cos\theta_B \ .
\end{aligned}$$

If $\hat{\mu}(0)$ is the unit vector along the initial spin direction of the muon

$$\hat{\mu}(0) = \hat{x} = \hat{x}'\cos\theta_B\cos\phi_B - \hat{y}'\sin\phi_B + \hat{z}'\sin\theta_B\cos\phi_B \ .$$

At later times, $\hat{\mu}$ will precess around $\hat{z}'$ with angular frequency ω:

$$\begin{aligned}
\hat{\mu}(t) = \ & \hat{x}'(\cos\omega t\cos\theta_B\cos\phi_B + \sin\omega t\sin\phi_B) + \\
& \hat{y}'(\sin\omega t\cos\theta_B\cos\phi_B - \cos\omega t\sin\phi_B) + \\
& \hat{z}'\sin\theta_B\cos\phi_B \ .
\end{aligned}$$

In spectrometer coordinates this would be

$$\begin{aligned}
\hat{\mu}(t) = \ & \hat{x}\left[\cos\omega t + \sin^2\theta_B\cos^2\phi_B(1-\cos\omega t)\right] + \\
& \hat{y}\left[(1-\cos\omega t)\sin^2\theta_B\cos\phi_B\sin\phi_B + \sin\omega t\cos\theta_B\right] + \\
& \hat{z}\sin\theta_B\left[(1-\cos\omega t)\cos\theta_B\cos\phi_B - \sin\omega t\sin\phi_B)\right] \ .
\end{aligned}$$

Consider now a decay positron whose polar and azimuthal angles in the spectrometer, θ_a and ϕ_a, are such as to allow acceptance. The positron's unit direction vector is then given by

$$\hat{e} = \hat{x}\sin\theta_a\cos\phi_a + \hat{y}\sin\theta_a\sin\phi_a + \hat{z}\cos\theta_a \ .$$

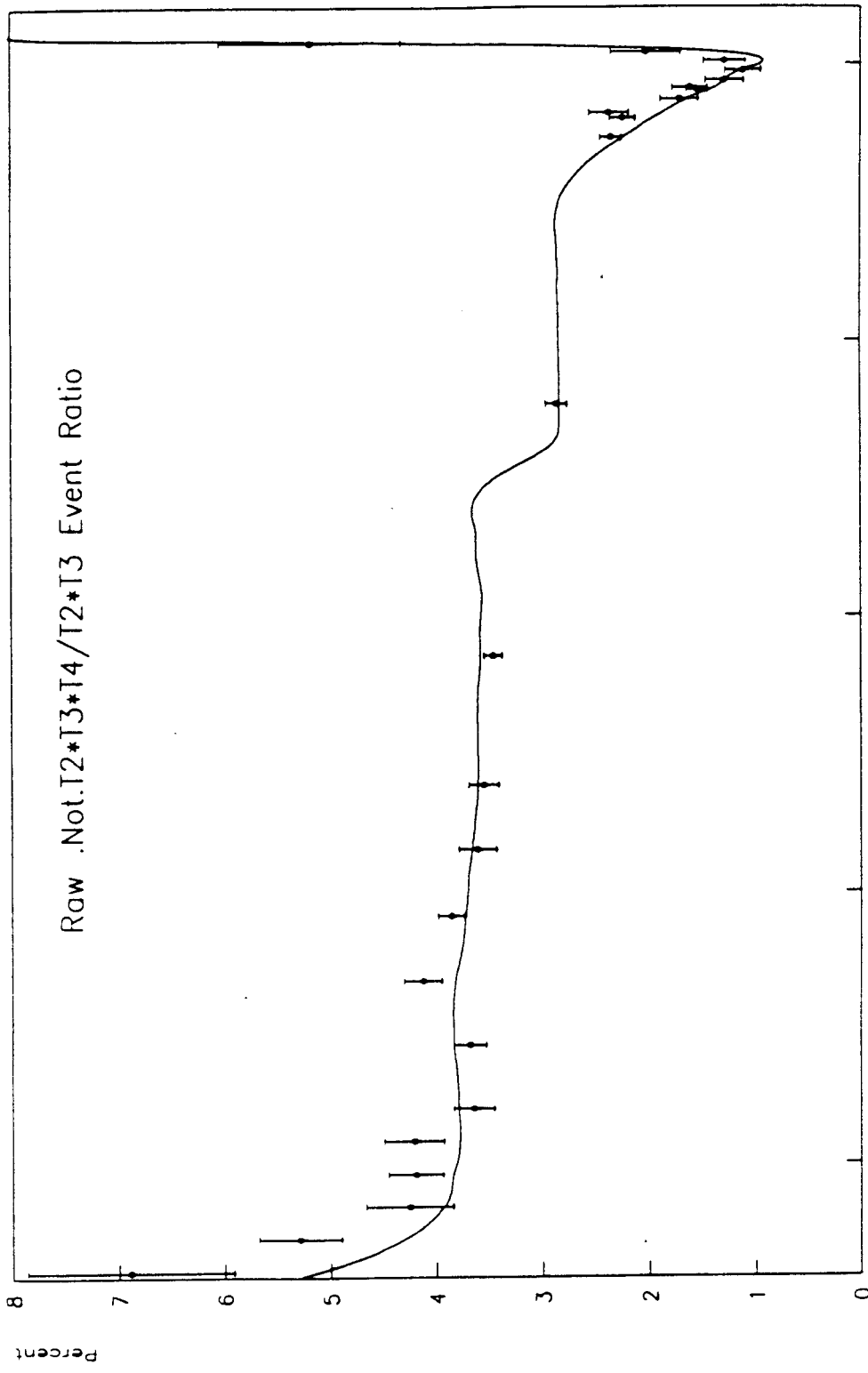

Figure 28. Comparison of the measured and calculated $T2 \cdot T3/\overline{T2} \cdot T3 \cdot T4$ ratio. The calculation is from first principles; the measured points are shown with only the statistical errors of the data.

This result can be used to find, for example, the spectrum distortion that could result from the target not being centered in the magnetic field of Comus. From field measurements,

$$\sin\theta_B = (0.0244\,\mathrm{cm}^{-1})r$$

at the target position for small radial displacements, r. Applying this measurement to the above results,

$$\frac{\Delta\mathcal{P}(x)}{\mathcal{P}(x)} < \alpha(x)\frac{0.0244}{\mathrm{cm}}r\ .$$

A.2 Misaligned Muon Spin

Consider now another possibility—that the muon spin is not quite along the $\hat{x}$ direction as assumed, but is at an angle ϵ from the $\hat{x}$-$\hat{y}$ plane. This might, for example, arise from misalignment of the spectrometer with respect to the beam line. (Deviations which are not out of that plane make no difference.) It will be assumed that no other asymmetries exist: that the spectrometer acceptance is azimuthally symmetric and the magnetic field at the target is uniform and along $\hat{z}$. In the same notation as Section A.1,

$$\hat{\mu}(t) = \hat{x}\cos\omega t\cos\epsilon + \hat{y}\sin\omega t\cos\epsilon + \hat{z}\sin\epsilon\ .$$

Then the angle between the muon spin and an accepted positron is given by

$$\cos\gamma(t) \equiv \hat{\mu}(t)\cdot\hat{e} = \sin\theta_a\cos\epsilon\,(\cos\phi_a\cos\omega t + \sin\phi_a\sin\omega t) + \cos\theta_a\sin\epsilon\ ,$$

which leads us to the equation

$$\begin{aligned}\mathcal{P}(x) &\propto \int_0^\infty \tfrac{dt}{\tau}\exp(-\tfrac{t}{\tau})\int_{\theta_1}^{\theta_2}\sin\theta_a d\theta_a\int_0^{2\pi}[1+\alpha(x)\cos\gamma(t)]\,d\phi_a \\ &\propto A\,[1+\alpha(x)<\cos\theta_a>\sin\epsilon]\ .\end{aligned}$$

There is, of course, no dependence upon ω in this equation since the angle between the muon spin and the spectrometer acceptance is constant; any distortion of the spectrum would arise from the energy-dependence of $\alpha(x)$. For the Comus spectrometer, again using $<\cos\theta_a>\approx 1$, the upper limit on the fractional error is then obtained as

$$\frac{\Delta\mathcal{P}(x)}{\mathcal{P}(x)} \leq \alpha(x)\sin\epsilon\ .$$

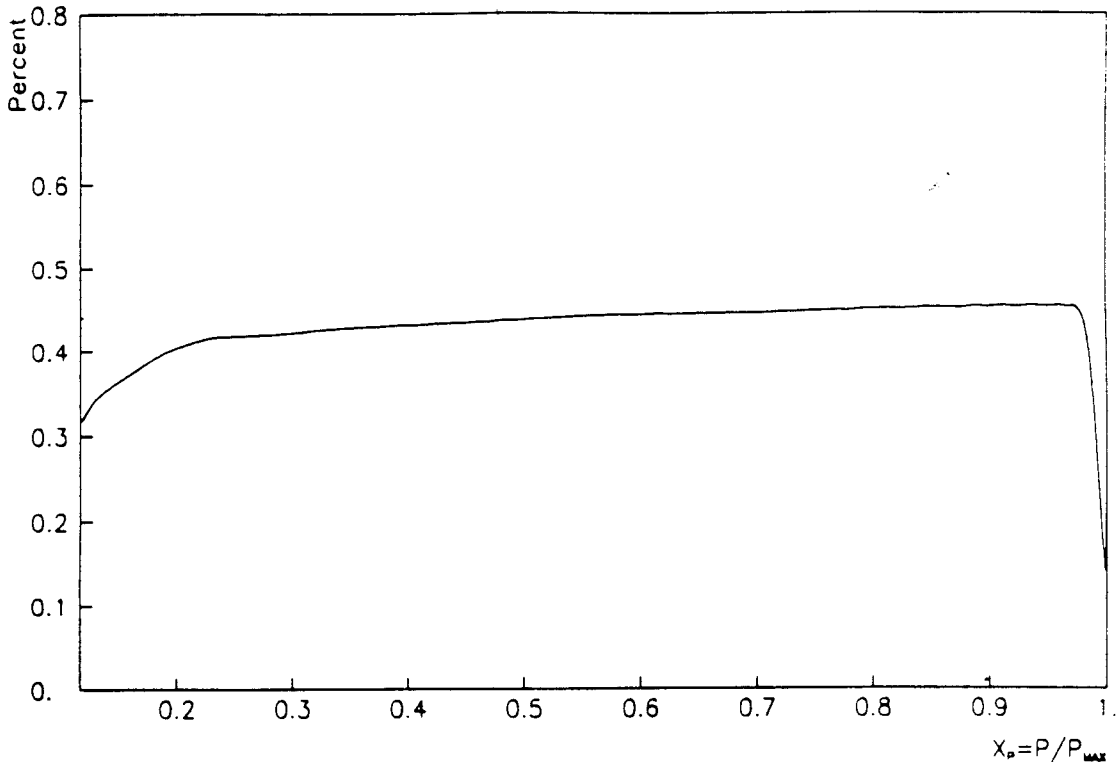

Figure 26. Relative spectrum effect of scatters from $C2$, as calculated by Monte Carlo. The dip near $x_p = 1$ arises from the number of particles on $C2$ falling off more rapidly than the number accepted, since $C2$ forms part of the high side of the momentum selection slit.

such as the aforementioned light guide on $C1$ would not be much of a problem anyway: the fractional spectrum distortion at $x = 0.1$ is only a negligible 0.005% for a muon polarization of 0.25. In fact, any reasonable effort to produce an azimuthally uniform acceptance would avoid problems in this particular experiment.

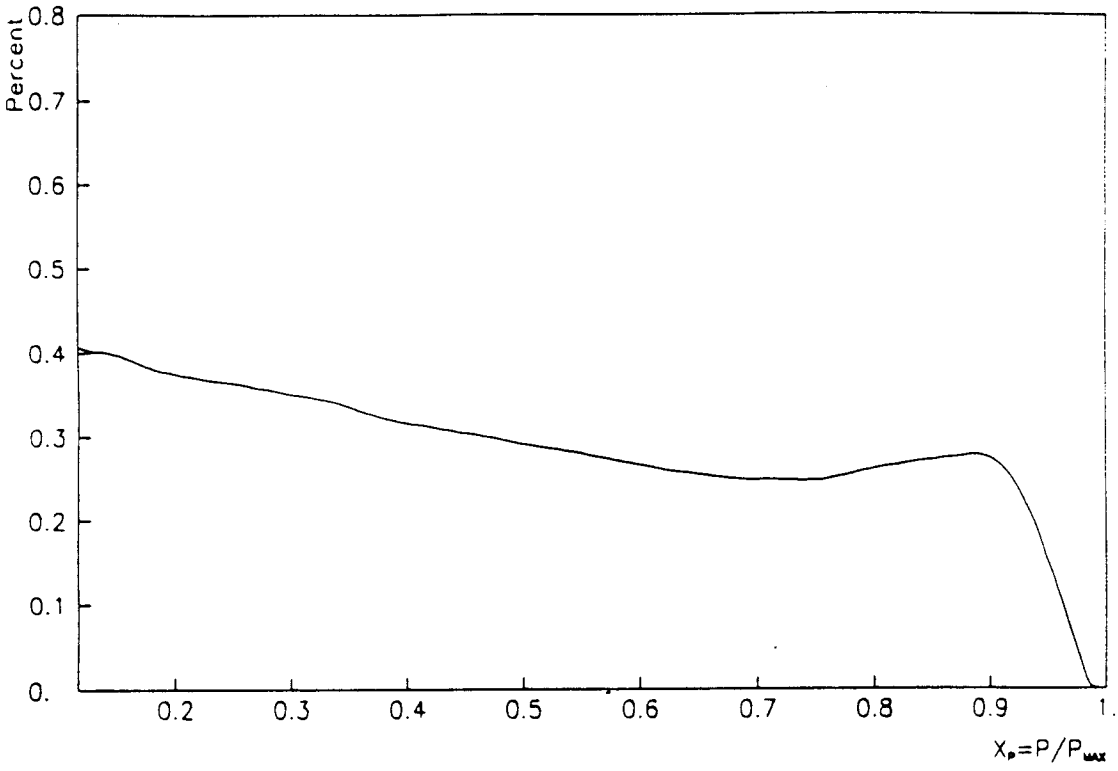

Figure 24. Relative spectrum effect of scatters from the bevel of the $K3$ collimator, as calculated by Monte Carlo. The drop for $x_p > 0.9$ is due to the absence of incident particles from above the endpoint momentum.

are four conditions imposed on the field derivatives by Maxwell's equations:

$$\vec{\nabla} \cdot \vec{B} = 0$$

$$\vec{\nabla} \times \vec{B} = 0 \, .$$

The remaining derivatives to eliminate at the probe center are

$$\frac{\partial B_x}{\partial x} = \frac{\partial B_x}{\partial y} = \frac{\partial B_x}{\partial z} = \frac{\partial B_z}{\partial y} = \frac{\partial B_z}{\partial z} = 0 \, .$$

Several of these conditions could be achieved through the symmetries of the magnet. With right-handed Cartesian coordinates $\hat{x}$,$\hat{y}$,$\hat{z}$, whose origin is not on the magnet's axis, $\hat{x}$ is defined to be tangential to a circle around the symmetry axis, $\hat{y}$ to be radially inward and $\hat{z}$ to be parallel to the symmetry axis. Then, because Comus is axially symmetric with no significant azimuthal field components, $B_x = 0$ at $x = 0$ and, therefore,

$$\frac{\partial B_x}{\partial y} = \frac{\partial B_x}{\partial z} = 0 \, .$$

One more condition can be satisfied by appropriately choosing the value of z at which the probe is placed. If B_r is the radial field component at a distance r from the symmetry axis, then

$$\frac{\partial B_x}{\partial x} = \frac{B_r}{r} \, .$$

Thus, this derivative vanishes where $B_r = 0$, which will be true for some z near the spectrometer midplane at any radius—for a spectrometer which is nearly symmetric across this midplane.

Alternatively, one could choose a value of z at which there was an extremum in B_z, thereby eliminating $\partial B_z/\partial z$. Both this and the $B_r = 0$ condition would be fulfilled at a single point if the magnet were completely symmetric across the midplane, but this was not quite true for Comus. Forced to choose which of the two conditions to satisfy, one should note that it is much easier to act upon two derivatives of the same field component for engineering reasons. Thus, z was chosen such that

$$\frac{\partial B_x}{\partial x} = 0$$

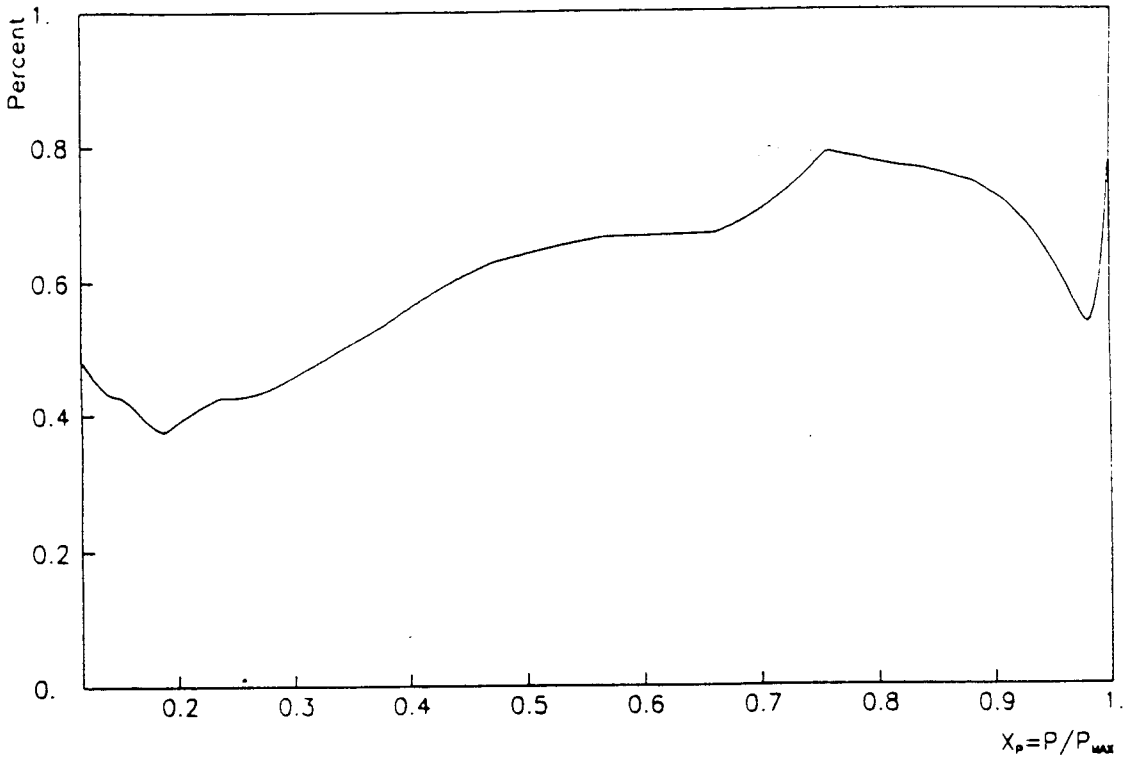

Figure 22. Relative spectrum effect due to the three upstream sets of collimator-suspension cables, as calculated by Monte Carlo. The reduced effect above $x_p = 0.75$ is due to the absence of particles incident on the cables from above the spectrum endpoint, while the rise near $x_p = 1$ is due to the drop in the number of normal events near the endpoint.

size. Since the surface area available for passive cooling scales as b^2, while the heat produced for a given gradient compensation scales as, at least, b^4, this is clearly desirable.

B.2.2 Canceling $\frac{\partial B_z}{\partial y}$

The procedure for canceling this gradient is similar. Again, the field is found at $(0,0)$ from four filaments placed at $(\pm a, \pm b)$, except that they now all carry a current I in the -$\hat{x}$ direction. B_z and all its even derivatives with respect to y vanish, while

$$\frac{\partial B_z}{\partial y} = \frac{2}{b^2}\frac{\mu_0 I}{\pi}\frac{q^2-1}{(1+q^2)^2} \qquad \text{and} \qquad \frac{\partial^3 B_z}{\partial y^3} = \frac{12}{b^4}\frac{\mu_0 I}{\pi}\frac{1-6q^2+q^4}{(1+q^2)^4}\ .$$

Much as before, the higher derivatives can be ignored and several values of q can be chosen which, taken together, minimize $\partial^3 B_z/\partial z^3$ and maximize $\partial B_z/\partial z$. Again, one should try to minimize b.

B.3 Other Considerations

When the absolute size of the gradients to be compensated is large, substantial current densities are required in the compensating coils. As an example, when Comus was tuned to the muon decay endpoint, $\partial B_z/\partial y = 220$ gauss/cm. About 60 amps were required to cancel this gradient in the coils built for this experiment. While the absolute size of the current stems from the use of only four sets of conductors (which maximized the conductor filling factor and simplified the conductor positioning), the current density would be high for any design and implies substantial heating. It is for this reason that printed circuit techniques[2] were rejected in favor of a machined coil form and #14 copper wire. Even then, forced air cooling was required.

[2]The printed circuit compensating coils discussed by K. Borer and G. Fremont for use with the CERN NMR probes were rated at 20 gauss/cm; these probes are substantially thinner than the LBL-designed probes and compensation therefore requires less current.

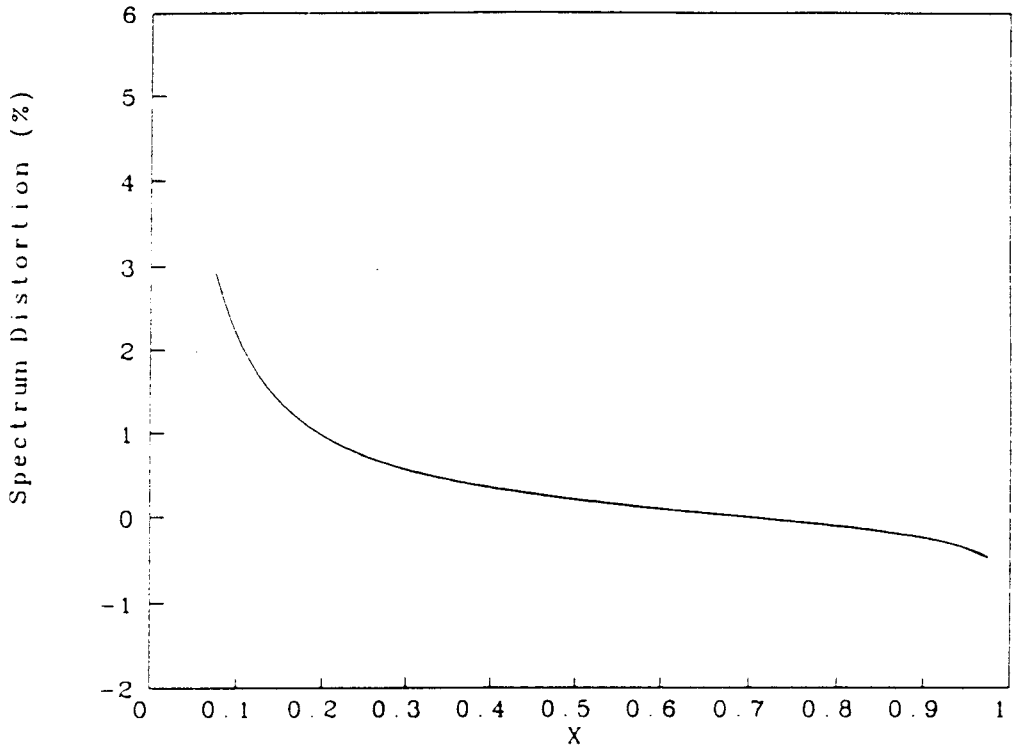

Figure 20. Relative effect on the spectrum of external bremsstrahlung in $T1$.

Appendix C

Monte Carlo Physics — EGS

C.1 Introduction to EGS

The EGS4 Code System[1] is a general purpose program for the simulation of electromagnetic showers. It extends the capabilities of, and corrects errors in, EGS3.[2] This latter code was used in the earlier part of the analysis of this experiment, until EGS4 was released and could be implemented. The total dynamic kinetic energy range is claimed to be from a few tens of KeV to a few thousand GeV for charged particles and from 1 keV to a few thousand GeV for photons. This covers the energy range with which a muon decay experiment is likely to concern itself. The relevant physics are largely contained within this code system, with the user being mostly required to initialize the particle characteristics and trajectories, to handle of the geometry for particle propagation and to extract information from the particle showers. For high-quality results, the user must also carefully choose various parameters (such as thresholds for discrete particle treatment), balancing CPU time requirements against accuracy.

Given the historical development of EGS for medical physics and high-energy calorimetry, it is not surprising that time is not handled in the program at all. This means, barring

[1] W. R. Nelson, H. Hirayama and D. W. O. Rogers, SLAC **265** (1985).

[2] R. L. Ford and W. R. Nelson, SLAC 210 (1978).

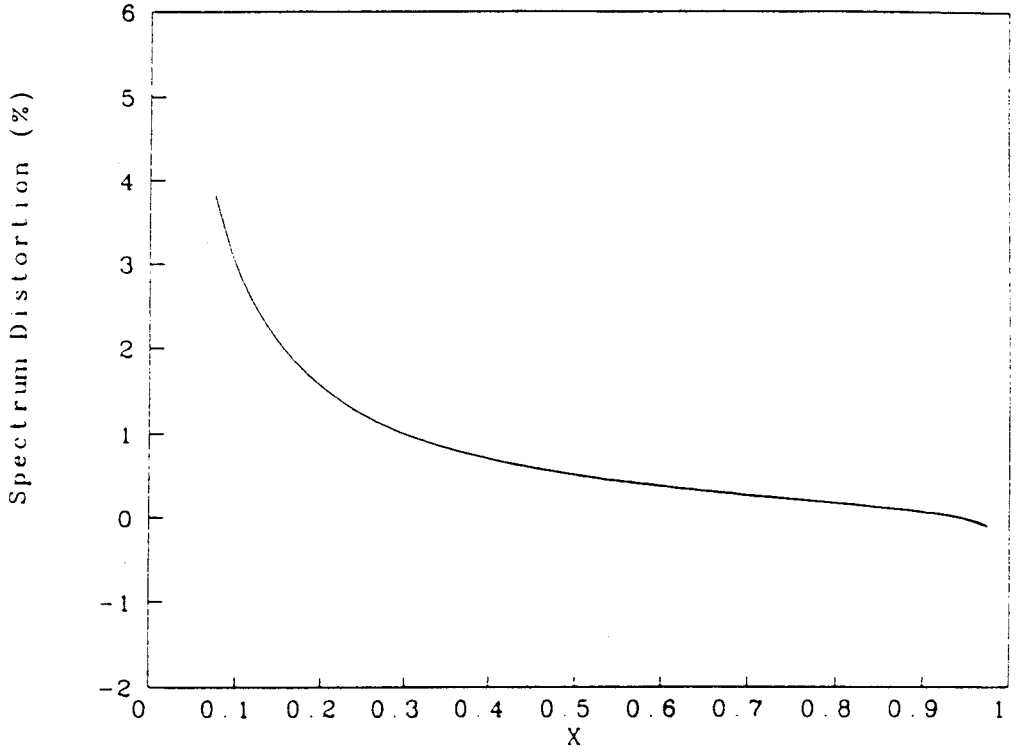

Figure 18. Relative effect on the spectrum of continuous energy losses in $T1$.

a counter, though there are also many examples among the physical processes which the particles undergo.

In such a situation, one would like to propagate a particle over a fairly long step and choose the energy loss from a known distribution depending on the incident particle's characteristics, the material and step size. This is easily implemented: EGS provides the average energy loss and one need only randomly choose a value from the energy-loss distribution whose average is equal to this. The particular one chosen was the Blunke-Leisegang distribution, which is somewhat broader and more accurate than the Landau distribution for thin lamina, becoming very similar for thick lamina. It is composed from the sum of four Gaussian curves whose relative weights, widths and centroids were chosen from empirical data. In order to choose a properly weighted variable from this distribution, one need only choose which of the four Gaussians to use, based on their relative weights, and then randomly sample from a Gaussian of this width and centroid.

There are, in general, problems of internal consistency with this approach, appearing in some dependence of the energy-straggling width on the step sizes taken to travel a given distance. This arises from the fact that the tails of distributions like that of Landau or Blunke-Leisegang do not join smoothly with the discrete energy-loss distribution; the tails are not of the correct shape and include energy losses past the threshold for discrete production. The distributions are accurate only in the region around the average energy-loss peak. Nonetheless, straggling can be incorporated in this way with reasonable accuracy, provided that the step size is small enough that the tail of the continuous loss distribution does not extend significantly past the discrete treatment threshold and that a trajectory through a region is not heavily subdivided. Also, errors are usually partially corrected by folding the energy-loss distribution with a resolution curve to reproduce the measured width of the ADC of a counter.

Another potential problem is the choice of the threshold for discrete production. If this threshold is too low, the calculation becomes hopelessly time-consuming, while, if too high, the real particles may escape from a thin lamina (such as $T1$) and cause effects (such

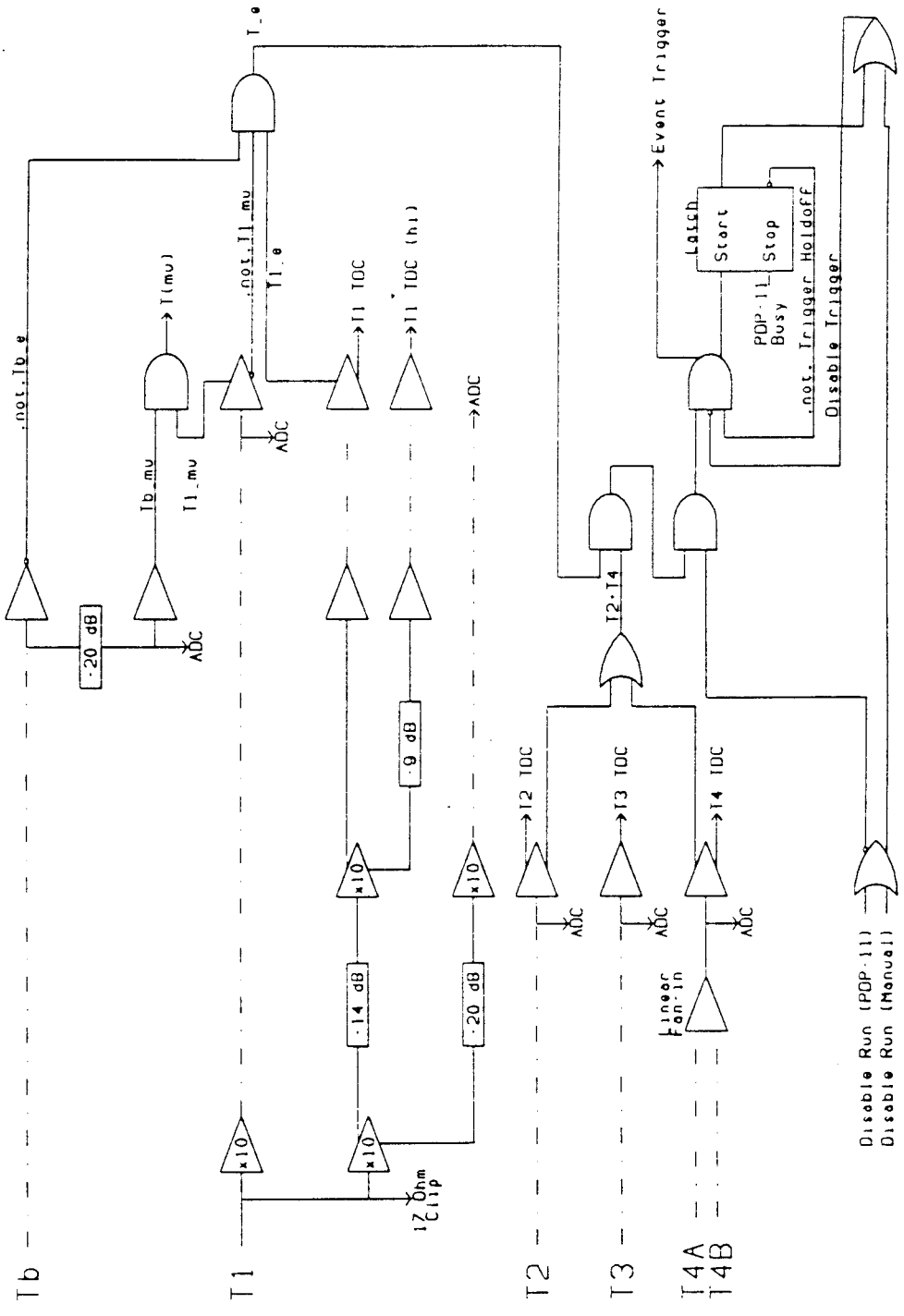

Figure 16. The trigger electronics, slightly simplified. Unlabled triangles represent discriminators. The electronics to the left of the dot/dash lines were in the experimental area, with the remainder in the counting room.

in the Monte Carlo simulation until after the first path length has been traversed, the scattering may not be relevant any more—enough energy may have already been deposited in the calculation to produce an event "veto".

- If a charged particle is travelling close to, and nearly parallel to, a material boundary, the calculated results can depend strongly upon the path-length limit. The reason, of course, is that a tiny scattering may allow the particle to escape from the region in a much shorter distance than would be needed if a straight path were followed. One place where this problem arises is in the scattering of grazing incidence particles from collimators. Another is in the muon-stopping target, $T1$, which is very thin compared to its height and width; some of the e^+ will be produced with initial trajectories nearly in the target plane, but can occasionally scatter into the spectrometer acceptance. EGS will naively move particles a distance of a centimeter or more before considering the possibility of a scatter, while the real particles will often scatter out of the target well before that distance and, thus, be scattered at smaller angles than found by EGS. For these reasons, EGS may give erroneous values for both the energy deposition in the target and the likelihood of a particle scattering into the spectrometer acceptance, unless one stringently limits the allowable path length per step.

A package of macros referred to as PRESTA[6] is available to improve the particle transport in EGS4. In addition to including a boundary crossing and lateral transport algorithm, so that the above problems are more accurately handled, it handles the multiple scattering path-length correction in a way that is consistent with the multiple scattering treatment. This means that results are nearly independent of step size—which is not always the case with uncorrected EGS4 at low energy.

Most of the programs used to simulate the Comus spectrometer incorporated PRESTA. This macro package was generalized to allow region-by-region adjustment of the algorithm, increasing the speed and/or accuracy in most applications.

[6] Alex F. Bielajew and David W.O.Rogers, Report PIRS 042, 1986.

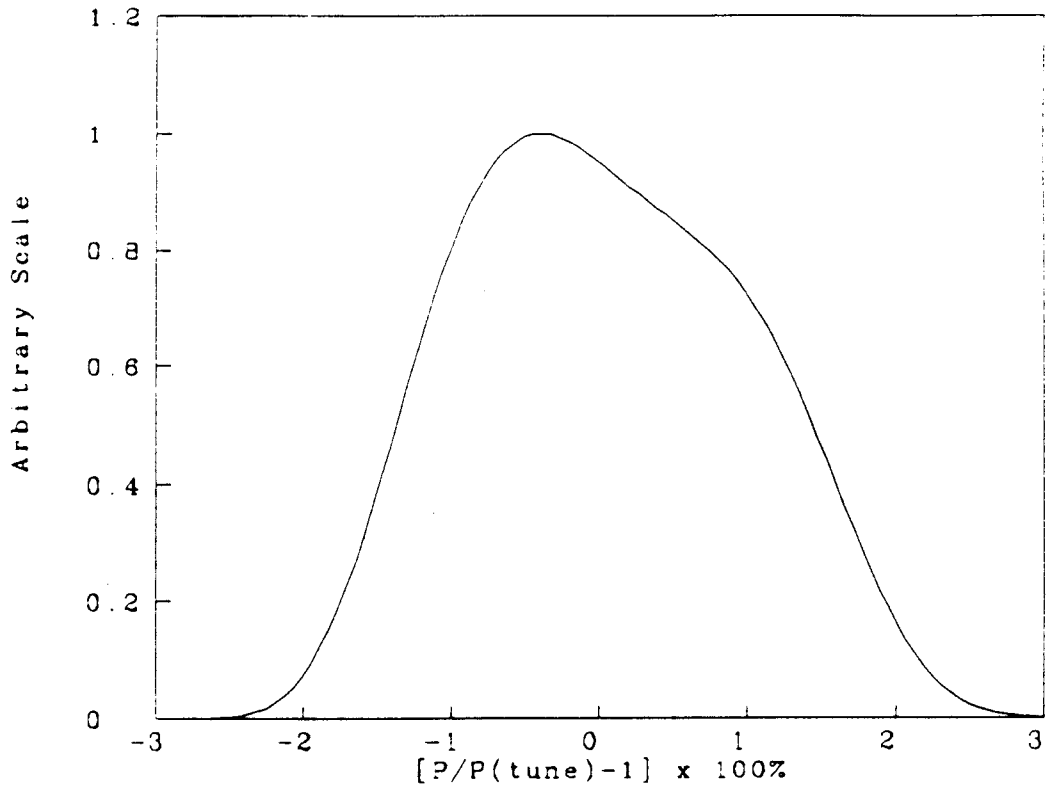

Figure 14. Calculated line shape of Comus spectrometer at $T1$. Note the break in the slope of the high momentum edge from the use of two separate collimators ($K3$ and $C2$).

impact in this experiment; bremsstrahlung, though, is important.

While the relative inaccuracy is small for heavy elements (nuclear bremsstrahlung being larger by a factor of $O(Z)$), the distinction between the two processes can be important for materials containing only light elements. Plastic scintillator, in which carbon ($Z = 6$) is the heaviest component, is a potential problem. This is especially true for low-energy primaries, for which the electron to nuclear ratio is much less than the high-energy limit. Thus, EGS4 has been modified to treat bremsstrahlung in the field of electrons more accurately, using a table of cross sections found from numerical integrations of a formula derived by E. Haug[7], which is too lengthy to justify its inclusion here. Also incorporated were the suggestions of the ICRU[8] with regard to the treatment of the shielding problem and the formula's applicability to e^+ above energies of 5 MeV, since Haug's result is, strictly speaking, applicable only to the scattering of two free e^-.

In this way EGS4 was given the correct stopping power due to bremsstrahlung in the electron field, but this was still done with a multiplicative correction factor to avoid extensive changes in the code. This is to say that the differential cross section was still not correct. For NE 110, hard bremsstrahlung was overemphasized by about 4.5%, while very soft bremsstrahlung was too small by as much as 17%.

Another thing to consider is that bremsstrahlung processes are not given the correct angular distributions for the final particle directions in EGS. In fact the lepton is not assumed to change direction when emitting bremsstrahlung, and the photon is always taken to be emitted at the same polar angle with respect to the lepton. The justification for the former, as given by the authors of EGS, is that multiple scattering dominates over the deflection from bremsstrahlung. In materials thicker than about 0.0025 radiation lengths, this is true. Fortunately, the absolute values of the angles involved are small enough that there is no significant effect in this experiment even when this condition is not met. The use of the average for the photon angle also presents no problem: the angles involved are

[7] E. Haug, Z. Naturforsch **30a**, 1099 (1975).

[8] International Commission on Radiation Units and Measurements, Report 37 (1984).

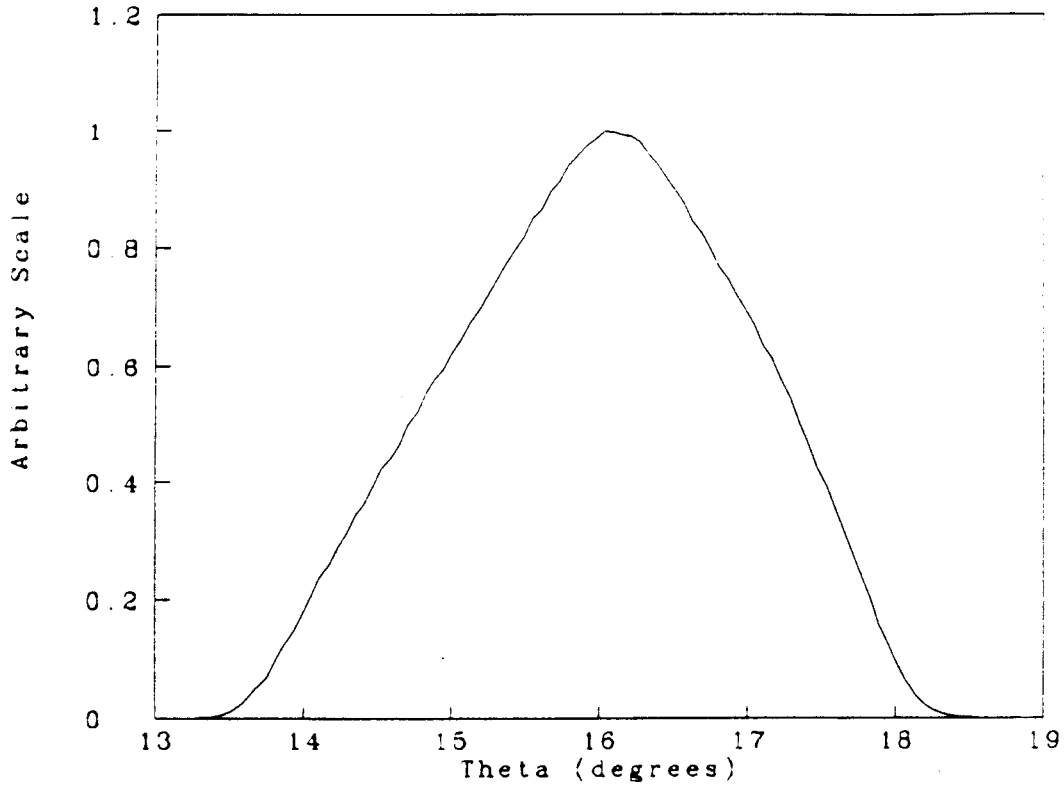

Figure 12. Calculated angular acceptance, averaged over momenta, of the Comus spectrometer at $T1$.

C.6 Bhabha Scattering

The separate treatment of Bhabha scattering and bremsstrahlung in the field of an electron is fundamentally artificial, since Bhabha scattering is always accompanied by real photon emission (Bloch-Nordsieck argument) and electrons recoil from the passing of the virtual photon in bremsstrahlung. However, they are treated separately both in the literature and in EGS.

The radiative corrections can, in principle, have a large fractional effect on the cross section for Bhabha scattering. This is especially true for large energy transfers, since the energy carried off by real photons drives the cross section to zero.[12] Unfortunately, available calculations of the radiative corrections are not directly applicable to this experiment, having been done in the soft photon approximation,[13,14,15] for virtual photons only,[16] for ultra-relativistic energies,[17] for large energy transfers[18] or for specific experiments.

The Bhabha scatters of most importance to this experiment are those in which positrons of 20-53 MeV lose 10-50% of their energy to relatively low-energy electrons. The soft photon calculations predict reductions of a few percent, but have a photon energy cutoff in a logarithmic term and so do not give a definite prediction; plausible cutoffs yield reductions of 1-10%. The virtual photon calculations of Furlan and Peressutti predict a reduction of about 1% in the probability of Bhabha scatters for energy transfers of around 20%. The ultra-relativistic formula predicts a reduction of 5-6%, and, in the large energy transfer formula, the cross section is lowered by 10%. Thus, a reasonable estimate for the cross-section reduction is $(5 \pm 4)\%$.

---

[12] A. C. Hearn, P. K. Kuo and D. R. Yennie, Phys. Rev. **137**, 1950 (1969).

[13] A. I. Akhiezer and R. Polovin, Doklady Akad. Nauk USSR, **90**, 55 (1953).

[14] M. Redhead, Proc. Roy. Soc. (London) A **220**, 219 (1953).

[15] R. Polovin, JETP, **31**, 449 (1956), Sov. Phys. JETP, **4**, 385 (1957).

[16] G. Furlan and G. Peressutti, Nuovo Cimento **19**, 830 (1961).

[17] A. I. Akhiezer and V. B. Berestetskii, in *Quantum Electrodynamics* (Interscience Publishers, New York, 1965), p. 730.

[18] A. C. Hearn, P. K. Kuo and D. R. Yennie, Phys. Rev. **137**, 1950 (1969).

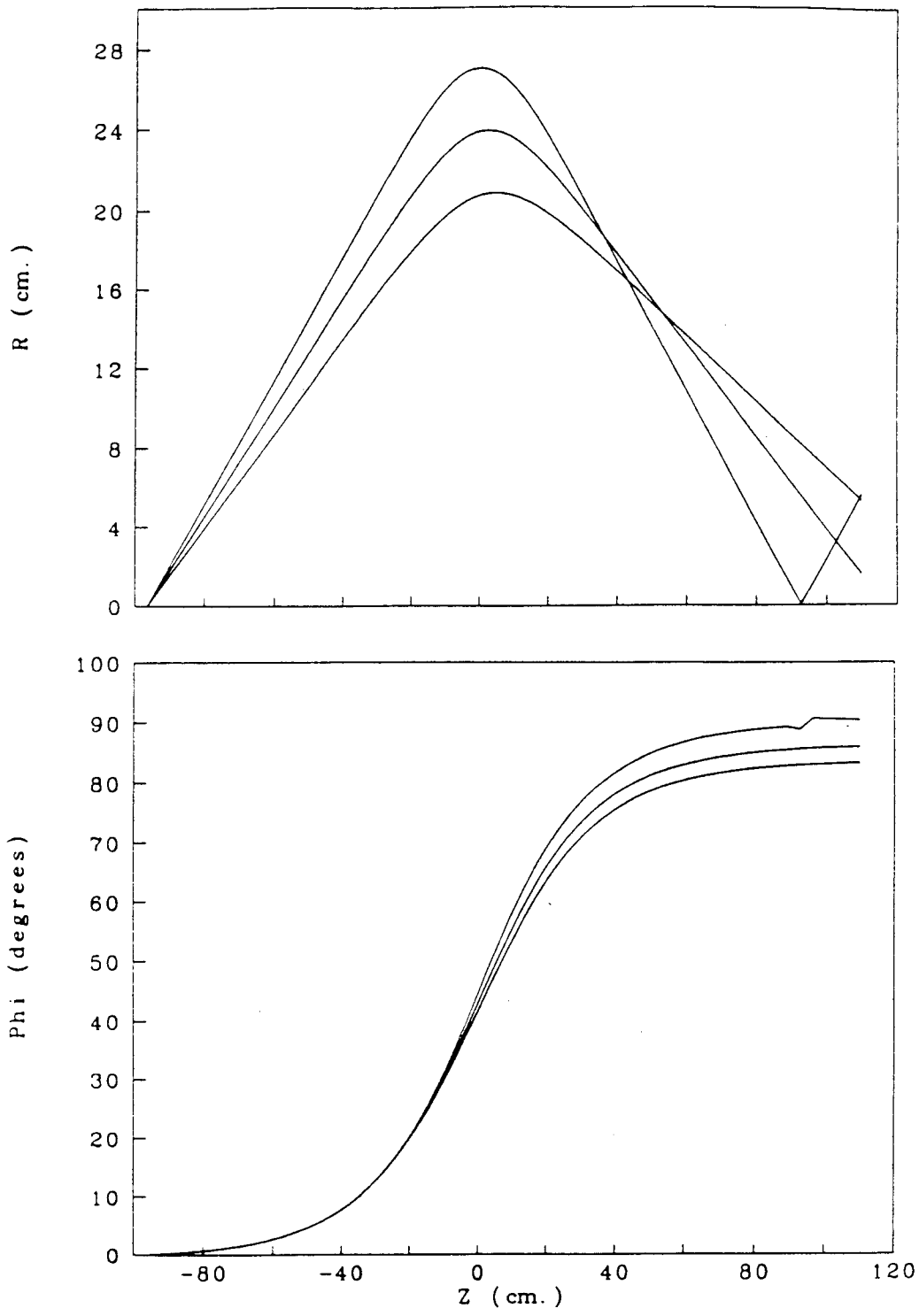

Figure 10. Typical accepted trajectories calculated for the Comus spectrometer. Note the approximate ring focus in the radial distribution.

0.5%. Based on Bethe's quantitative comparison with the exact theory of Goudsmit and Saunderson,[22] it does not appear that multiple scattering uncertainties at small angles should be important when the step sizes in EGS are not large.

One shortcoming in the EGS treatment that must be noted is this: scattering from atomic electrons below the threshold for discrete treatment is included as a multiplicative correction to Molière scattering, approximating the electrons as, basically, protons. This is obviously incorrect for scattering at angles of more than 90°. For a discrete treatment limit of 89 KeV kinetic energy, such as was typically used in running EGS, the maximum pseudo-elastic single scattering angle of 6 MeV positrons from electrons should actually be 2.8°. For 50 MeV positrons, the angle becomes 0.35°. The approximation can be significant in light materials, such as NE110, where single scatters at large angles are overstated by 17%. Fortunately, backscattering has fairly low probability in light materials. The primary effect in this experiment was to reduce the calculated detection efficiency slightly; this was corrected by hand.

Calculations of backscattering from active media (such as the $T3$ counter) are biased by another effect which is inherent in a condensed history Monte Carlo such as EGS. Particles are propagated a finite distance before "continuous" effects like multiple scattering are considered. This means that energy deposition by a backscattered particle in a scintillator will be overstated, since it usually results from a single nuclear scatter that occurred before the end of the step. Reducing step sizes near the surface, as is done by PRESTA, reduces the bias (but does not eliminate it, since the step sizes are not reduced below some finite limit). In principle, it would be nearly possible to eliminate this problem by treating single scatters of more than some cutoff angle as a discrete process to be included in the reaction cross section.

In their evaluation of the accuracy of the treatment of backscattering by PRESTA, Bielajew and Rogers[23] found that the fraction of energy reflected from a semi-infinite slab showed

[22] S. A. Goudsmit and J. L. Saunderson, Phys. Rev. **57**, 24 and **58**, 36 (1940).

[23] Alex F. Bielajew and David W.O.Rogers, Report PIRS 042, pp.29-30, 1986.

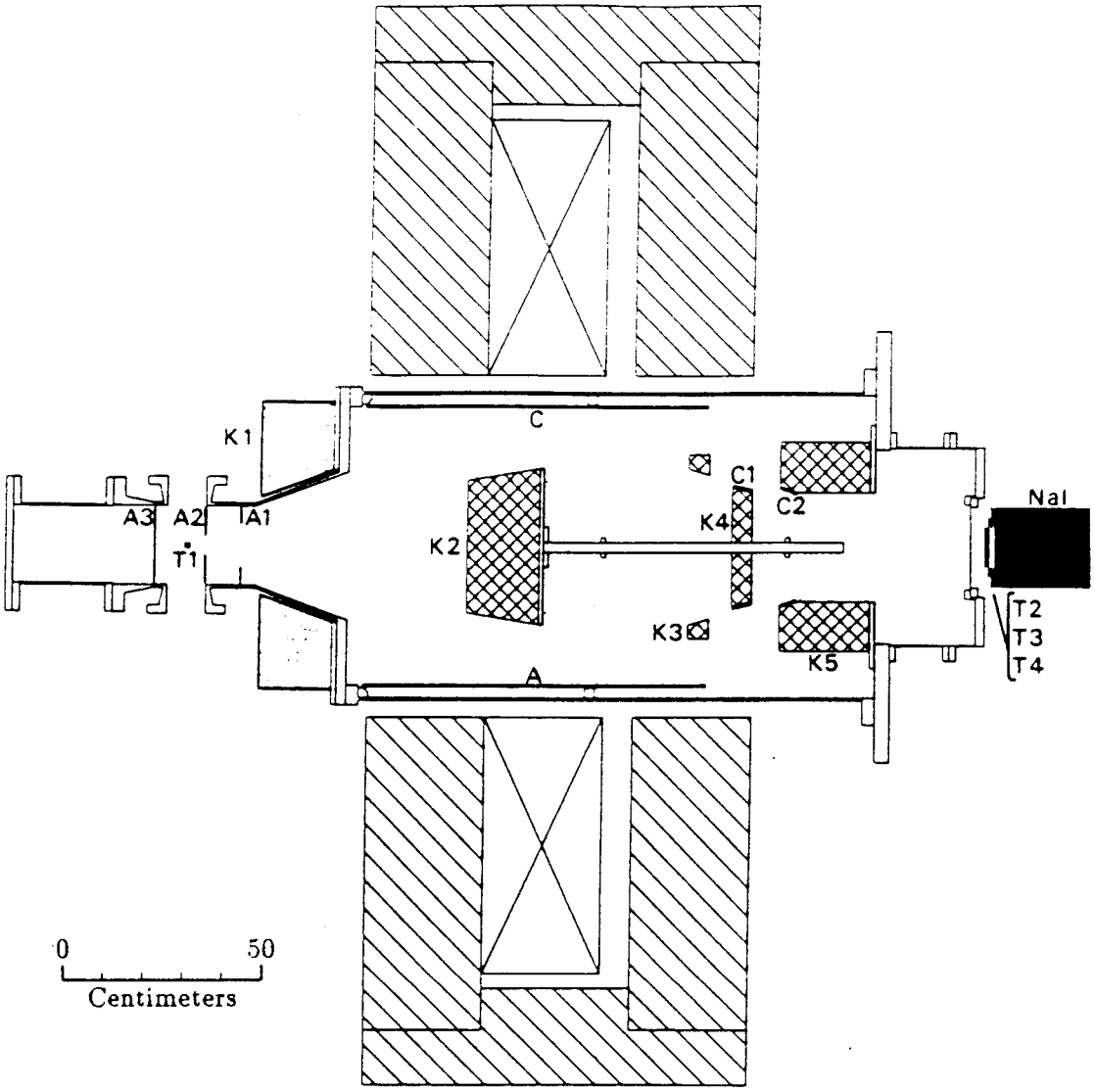

Figure 8. Vertical section through the Comus spectrometer. The dotted lines represent the collimator-support cables, projected onto this plane.

Appendix D

Monte Carlo Physics — TRIM

The stopping distribution of heavy particles for one special case—that of a fixed energy beam normally incident on a homogeneous, semi-infinite medium—is fairly well understood. However, analytic calculations are not generally applicable to real experiments; measurements find both shorter average ranges and asymmetric stopping distributions about the average because of large angle scattering. More complex geometries cause further complications.

Realistic stopping distributions can be obtained through Monte Carlo calculation. The TRIM85[1] code implements this for low-energy ions of hydrogen through uranium incident on a wide variety of materials. It must be noted, however, that the source code provided does not contain all of the features attributed to it; alternative versions were used to obtain some of the results shown in the book by Ziegler *et al.*

This code has been rewritten extensively, so as to apply it to the problem of a μ^+ stopping in a complex geometry. Geometrical, input and output routines are separated from the routines involved with physics, emulating the approach used in the EGS package. The physics in TRIM85 is improved as needed, including the insertion of intrinsic straggling and an iterative algorithm to find the energy loss during a step. The TRIM85 dE/dx values

[1] J. F. Ziegler, J. P. Biersack and U. Littmark, *The Stopping and Range of Ions in Solids* (Pergamon Press, New York, 1985) Vol. 1.

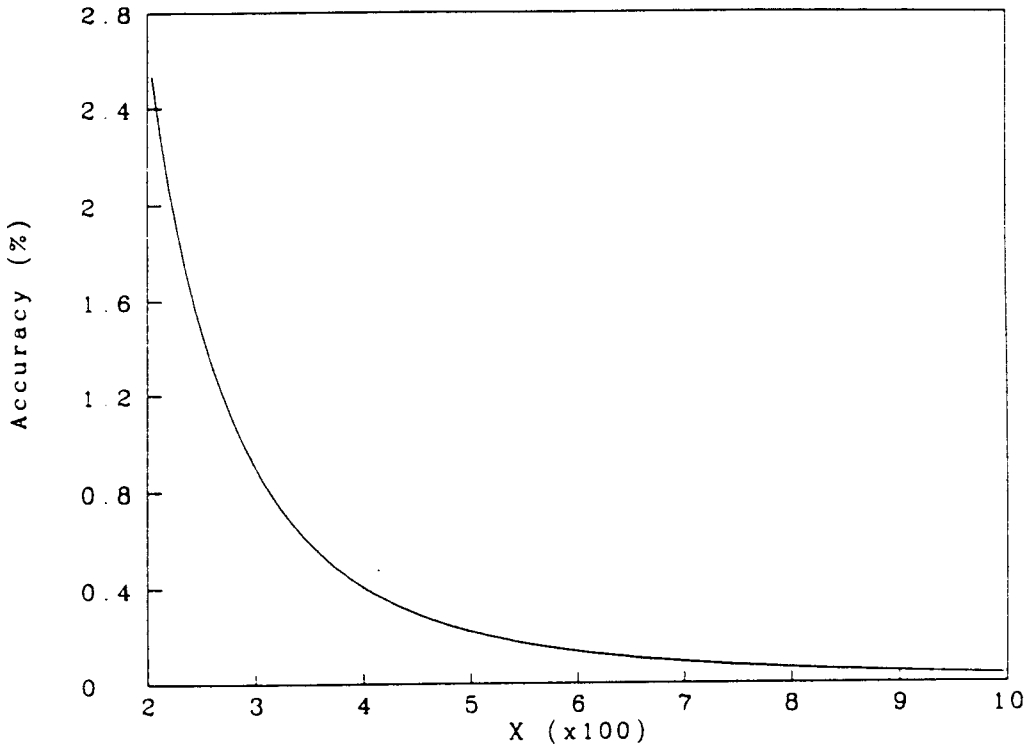

Figure 6. Relative accuracy of Grotch's approximate decay spectrum for use above $E_e > 3m_e$, relative to his exact first-order expression.

Appendix E

Systematic Effects

E.1 General Comments

Systematic errors in the determination of η are sensitive to the portion of the spectrum used in the fit, and, in an experiment where the amount of data gathered at any particular point on the spectrum is somewhat arbitrary, the errors are affected by the distribution of the statistics. For example, many systematics would have had dramatically more effect on the fitted value of η if data close to the endpoint had been used in the fit; effects which have a fairly uniform impact on the rest of the spectrum, such as errors in the calculated spectrometer line shape, may suddenly vanish at the endpoint and cause significant shape distortion.

Therefore, the systematic error estimates quoted for this experiment were usually determined by applying an effect to the spectrum, refitting the data to this modified spectrum and noting the shift in the fitted value of η. When an effect caused run-to-run variation at the same nominal spectrometer tune, this was inappropriate and a Monte Carlo approach was taken: for a number of separate fits to the spectrum, the effect was applied randomly to the data points, and the standard deviation of the resulting distribution of fitted η values was taken as the error.

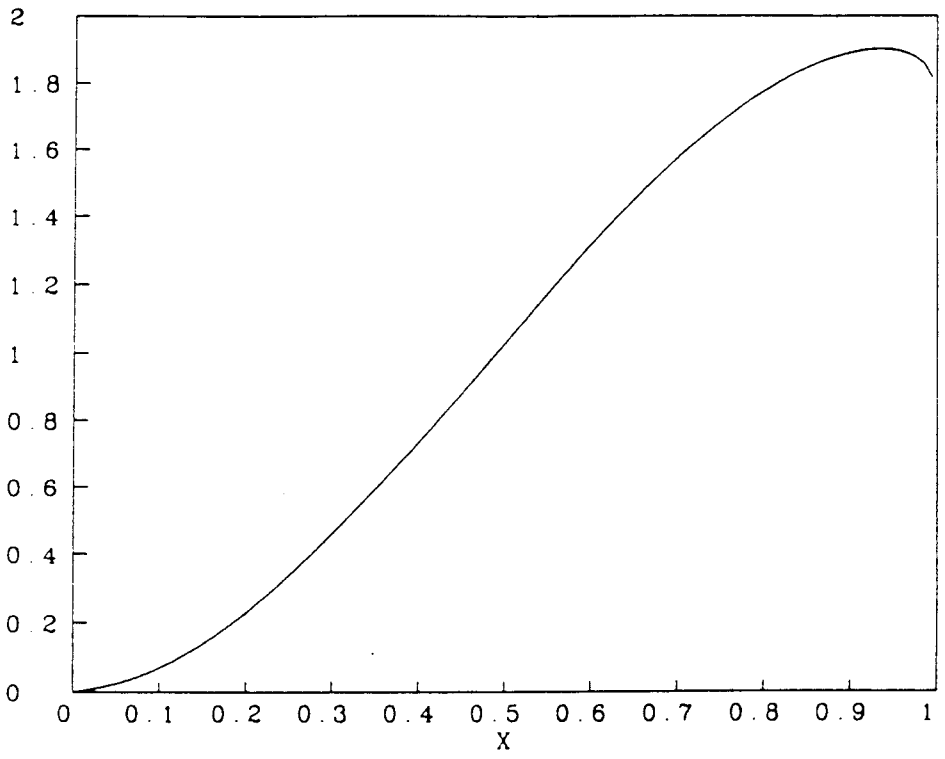

Figure 4. Positron energy spectrum from unpolarized muon decay, including radiative corrections. The spectrum is for $\rho = 3/4$, $\eta = 0$ and is normalized to 1.

collisions cause a shift of +0.212.

$T1$: Continuous Energy Loss Since the accuracy of the energy loss known for carbon at these energies is at the 0.9% level (Section C.2), the uncertainty in η from this is ± 0.002. With EGS4 there is also an inaccuracy of about 3% due to the soft radiative energy loss, and a 1% parameterization error, giving ± 0.008 in η.

Then, reserving the muon depth uncertainty to Section E.2.1, one calculational uncertainty is the exact beam spot distribution and, hence, the number of particles affected by the edges of $T1$ and the light guide that slightly overhangs the scintillator. Also, the 42° rotation of $T1$ means that particles entering one side of the spectrometer acceptance deposit more energy in $T1$ than those entering the other. Combined with a left-right asymmetry in the acceptance of about 5%, the average energy loss is shifted. Each of the above should affect the average energy loss by about a percent, giving an uncertainty in η of ± 0.004.

$T1$: Hard Interactions Bhabha scattering (Section 5.1.3 and Figure 19) and external bremsstrahlung (Section 5.1.4 and Figure 20) make large contributions to the effect that $T1$ has on the spectrum shape. The theoretical uncertainty (Sections C.6 and C.5) in the effect on η is about 4.5% or ± 0.009. In EGS4, there is a further uncertainty from the multiple scattering treatment, giving an error in η of ± 0.012.

The uncertainty in the calculation is estimated to be 8%, arising from the suppression of Bhabha scattering by the veto counters, counter calibrations and geometrical uncertainties. The resulting uncertainty in η is ± 0.017.

E.2.4 Detector Inefficiency

Uncorrected, this effect shifts the fitted value of η by -0.218. After the results have been approximately corrected for the shortcomings of EGS4 in annihilation (Section C.7) and backscattering (Section C.8) probabilities, the scattering treatment in EGS4 leaves an uncertainty in η of about ± 0.005.

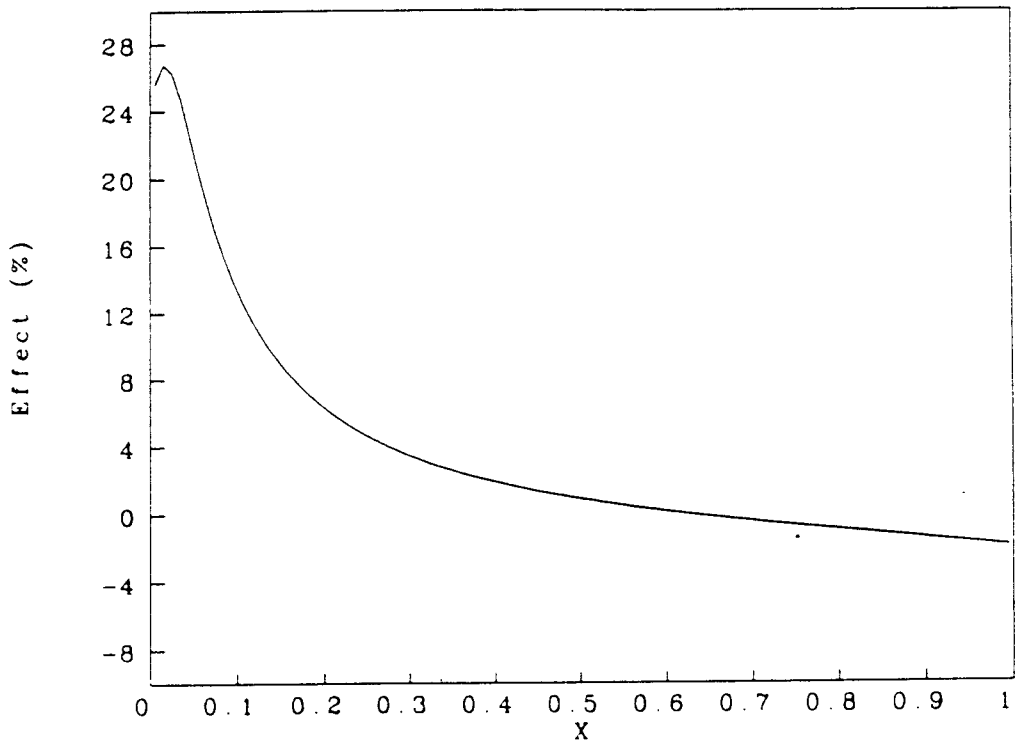

Figure 2. Relative sensitivity of the decay spectrum to η, as a function of x; radiative corrections are included and eliminate the divergence at $x = 0$.

E.2.7 $K2$

The theory accuracy for showering in thick lead is around 10%. EGS4 brings another 10% error from its handling of bremsstrahlung and annihilation in lead, and of multiple scattering in the aluminum shell. This gives ± 0.005 uncertainty in η from each. The calculational accuracy in η, due to approximations in the Monte Carlo and statistics, is ± 0.009.

E.2.8 $C1$

The EGS4 multiple scattering treatment is expected to give rather inaccurate answers for the scattering from the upstream face of $C1$; the error in this -0.010 effect on η is ± 0.002. The calibration accuracy on $C1$ is about 6%, giving an uncertainty of ± 0.004 in η from this. Geometry and Monte Carlo statistics give a further uncertainty of ± 0.008, for a total of ± 0.009.

E.2.9 Momentum Calibration

The most accurate spectrometer calibration relies on the spectrum endpoint. The saturation effects that appear in the magnet for $P_{tune} > 40$ MeV/c cause a 0.30% calculated nonlinearity of the magnetic monitors with respect to P_{tune} at the endpoint, as discussed in Section 6.4; since the accuracy of the calculated saturation effects is at the 10% level, an uncertainty of 0.03% remains after the calculated correction.

More importantly, the NMR and Hall probes used for magnetic monitoring (described in Sections 4.1.2 and B.4) began to disagree near the endpoint, leaving the absolute probe calibration in doubt by 0.1%. Adding these two errors in quadrature, the endpoint calibration accuracy is at the 0.11% level. The resulting inaccuracy in η is $\pm 0.008\%$.

E.2.10 Beam Centering

While the spectrometer solid angle is nearly constant over the $T1$ counter, the magnetic field varies somewhat in direction and can cause polarized muons to rotate about an axis

E.2.14 $C2$

The EGS4 multiple scattering treatment is expected to give rather inaccurate answers for the scattering from the bevel of $C2$; the error in this -0.008 effect on η is ± 0.002. The calibration accuracy on $C1$ is 12%, giving an uncertainty of ± 0.001 in η from this. Geometry and Monte Carlo statistics give a further uncertainty of ± 0.002, for a calculational error of ± 0.002.

E.2.15 Azimuthal Asymmetry

The spectrometer asymmetry, resulting from the double layer of scintillator on part of $C1$, $C1$'s traversal of the acceptance to connect to its light guide, the collimator-suspension cables, possible misalignment of collimators, and the ADC cuts in the $T1$ counter (which introduce some asymmetry because of $T1$'s rotation) is of the order of 10%. Using the results of Section A.3 to modify the spectrum for a 10% spectrometer asymmetry and a muon polarization of 25%, the effect on η turns out to be a negligible ± 0.001.

E.2.16 NMR Probe Cross-calibration

Since three separate NMR probes with overlapping ranges are used to span the spectrum, the relative calibration of the probes had to be measured to transfer the endpoint calibration. The highest to middle-range probes were cross-calibrated to 0.0030%, while the middle to lowest-range probes were cross-calibrated to 0.0015%. Choosing probe cross-calibrations randomly from Gaussians with these standard deviations, the resulting error in η was found to be ± 0.002.

E.2.14 $C2$

The EGS4 multiple scattering treatment is expected to give rather inaccurate answers for the scattering from the bevel of $C2$; the error in this -0.008 effect on η is ± 0.002. The calibration accuracy on $C1$ is 12%, giving an uncertainty of ± 0.001 in η from this. Geometry and Monte Carlo statistics give a further uncertainty of ± 0.002, for a calculational error of ± 0.002.

E.2.15 Azimuthal Asymmetry

The spectrometer asymmetry, resulting from the double layer of scintillator on part of $C1$, $C1$'s traversal of the acceptance to connect to its light guide, the collimator-suspension cables, possible misalignment of collimators, and the ADC cuts in the $T1$ counter (which introduce some asymmetry because of $T1$'s rotation) is of the order of 10%. Using the results of Section A.3 to modify the spectrum for a 10% spectrometer asymmetry and a muon polarization of 25%, the effect on η turns out to be a negligible ± 0.001.

E.2.16 NMR Probe Cross-calibration

Since three separate NMR probes with overlapping ranges are used to span the spectrum, the relative calibration of the probes had to be measured to transfer the endpoint calibration. The highest to middle-range probes were cross-calibrated to 0.0030%, while the middle to lowest-range probes were cross-calibrated to 0.0015%. Choosing probe cross-calibrations randomly from Gaussians with these standard deviations, the resulting error in η was found to be ± 0.002.

E.2.7 $K2$

The theory accuracy for showering in thick lead is around 10%. EGS4 brings another 10% error from its handling of bremsstrahlung and annihilation in lead, and of multiple scattering in the aluminum shell. This gives ± 0.005 uncertainty in η from each. The calculational accuracy in η, due to approximations in the Monte Carlo and statistics, is ± 0.009.

E.2.8 $C1$

The EGS4 multiple scattering treatment is expected to give rather inaccurate answers for the scattering from the upstream face of $C1$; the error in this -0.010 effect on η is ± 0.002. The calibration accuracy on $C1$ is about 6%, giving an uncertainty of ± 0.004 in η from this. Geometry and Monte Carlo statistics give a further uncertainty of ± 0.008, for a total of ± 0.009.

E.2.9 Momentum Calibration

The most accurate spectrometer calibration relies on the spectrum endpoint. The saturation effects that appear in the magnet for $P_{tune} > 40$ MeV/c cause a 0.30% calculated nonlinearity of the magnetic monitors with respect to P_{tune} at the endpoint, as discussed in Section 6.4; since the accuracy of the calculated saturation effects is at the 10% level, an uncertainty of 0.03% remains after the calculated correction.

More importantly, the NMR and Hall probes used for magnetic monitoring (described in Sections 4.1.2 and B.4) began to disagree near the endpoint, leaving the absolute probe calibration in doubt by 0.1%. Adding these two errors in quadrature, the endpoint calibration accuracy is at the 0.11% level. The resulting inaccuracy in η is $\pm 0.008\%$.

E.2.10 Beam Centering

While the spectrometer solid angle is nearly constant over the $T1$ counter, the magnetic field varies somewhat in direction and can cause polarized muons to rotate about an axis

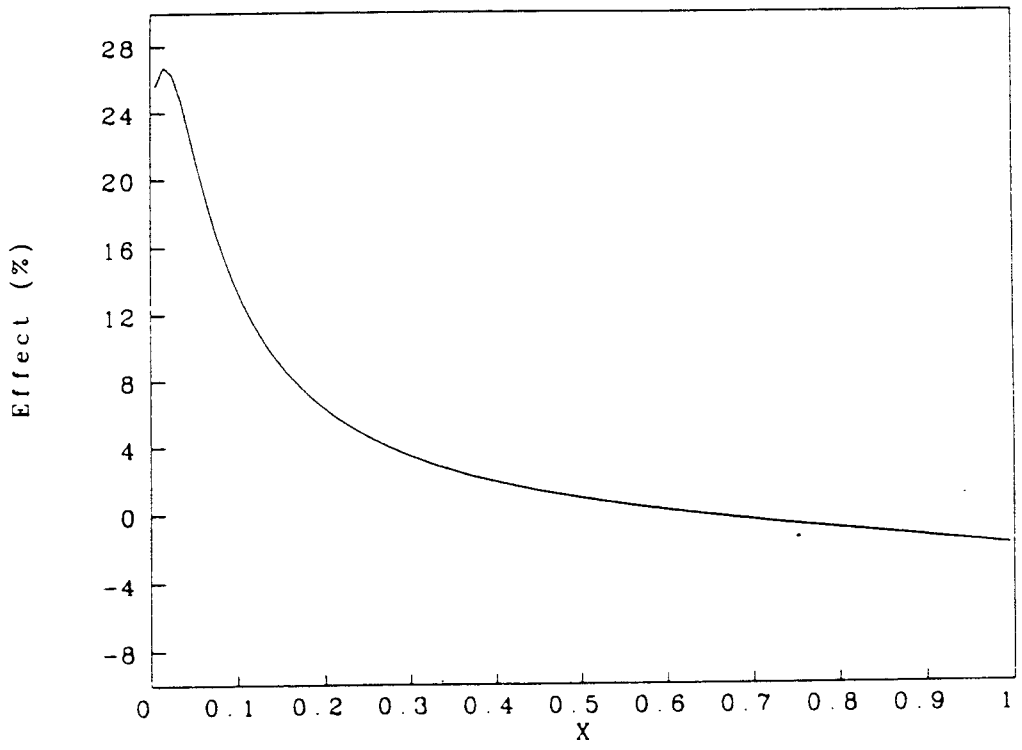

Figure 2. Relative sensitivity of the decay spectrum to η, as a function of x; radiative corrections are included and eliminate the divergence at $x = 0$.

collisions cause a shift of +0.212.

$T1$: **Continuous Energy Loss** Since the accuracy of the energy loss known for carbon at these energies is at the 0.9% level (Section C.2), the uncertainty in η from this is ± 0.002. With EGS4 there is also an inaccuracy of about 3% due to the soft radiative energy loss, and a 1% parameterization error, giving ± 0.008 in η.

Then, reserving the muon depth uncertainty to Section E.2.1, one calculational uncertainty is the exact beam spot distribution and, hence, the number of particles affected by the edges of $T1$ and the light guide that slightly overhangs the scintillator. Also, the 42° rotation of $T1$ means that particles entering one side of the spectrometer acceptance deposit more energy in $T1$ than those entering the other. Combined with a left-right asymmetry in the acceptance of about 5%, the average energy loss is shifted. Each of the above should affect the average energy loss by about a percent, giving an uncertainty in η of ± 0.004.

$T1$: **Hard Interactions** Bhabha scattering (Section 5.1.3 and Figure 19) and external bremsstrahlung (Section 5.1.4 and Figure 20) make large contributions to the effect that $T1$ has on the spectrum shape. The theoretical uncertainty (Sections C.6 and C.5) in the effect on η is about 4.5% or ± 0.009. In EGS4, there is a further uncertainty from the multiple scattering treatment, giving an error in η of ± 0.012.

The uncertainty in the calculation is estimated to be 8%, arising from the suppression of Bhabha scattering by the veto counters, counter calibrations and geometrical uncertainties. The resulting uncertainty in η is ± 0.017.

E.2.4 Detector Inefficiency

Uncorrected, this effect shifts the fitted value of η by -0.218. After the results have been approximately corrected for the shortcomings of EGS4 in annihilation (Section C.7) and backscattering (Section C.8) probabilities, the scattering treatment in EGS4 leaves an uncertainty in η of about ± 0.005.

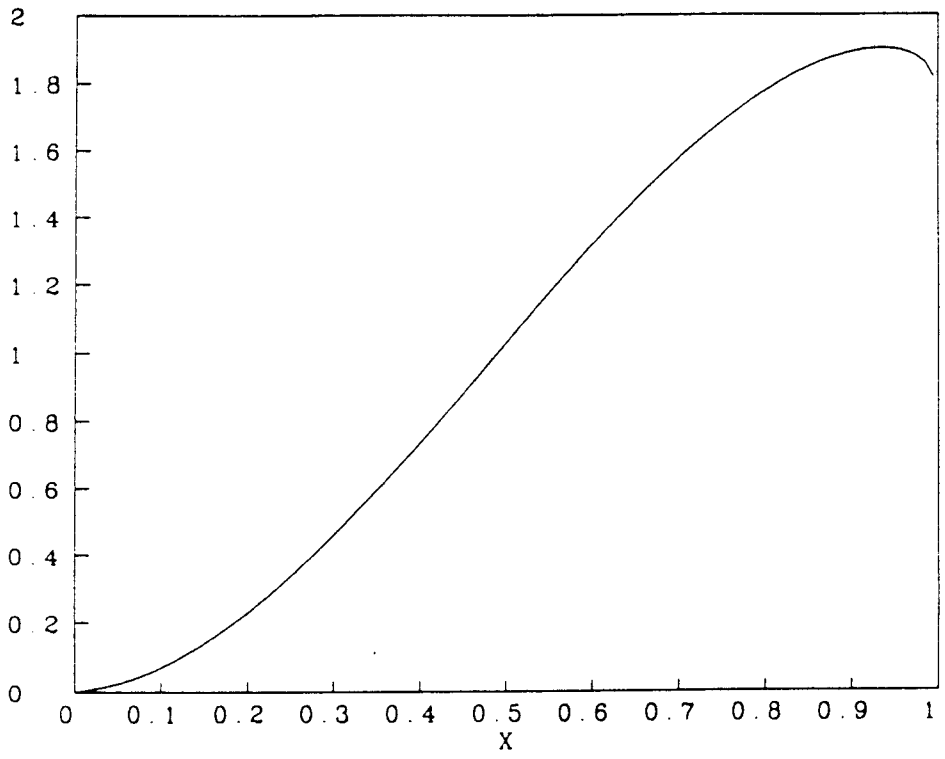

Figure 4. Positron energy spectrum from unpolarized muon decay, including radiative corrections. The spectrum is for $\rho = 3/4$, $\eta = 0$ and is normalized to 1.

Appendix E

Systematic Effects

E.1 General Comments

Systematic errors in the determination of η are sensitive to the portion of the spectrum used in the fit, and, in an experiment where the amount of data gathered at any particular point on the spectrum is somewhat arbitrary, the errors are affected by the distribution of the statistics. For example, many systematics would have had dramatically more effect on the fitted value of η if data close to the endpoint had been used in the fit; effects which have a fairly uniform impact on the rest of the spectrum, such as errors in the calculated spectrometer line shape, may suddenly vanish at the endpoint and cause significant shape distortion.

Therefore, the systematic error estimates quoted for this experiment were usually determined by applying an effect to the spectrum, refitting the data to this modified spectrum and noting the shift in the fitted value of η. When an effect caused run-to-run variation at the same nominal spectrometer tune, this was inappropriate and a Monte Carlo approach was taken: for a number of separate fits to the spectrum, the effect was applied randomly to the data points, and the standard deviation of the resulting distribution of fitted η values was taken as the error.

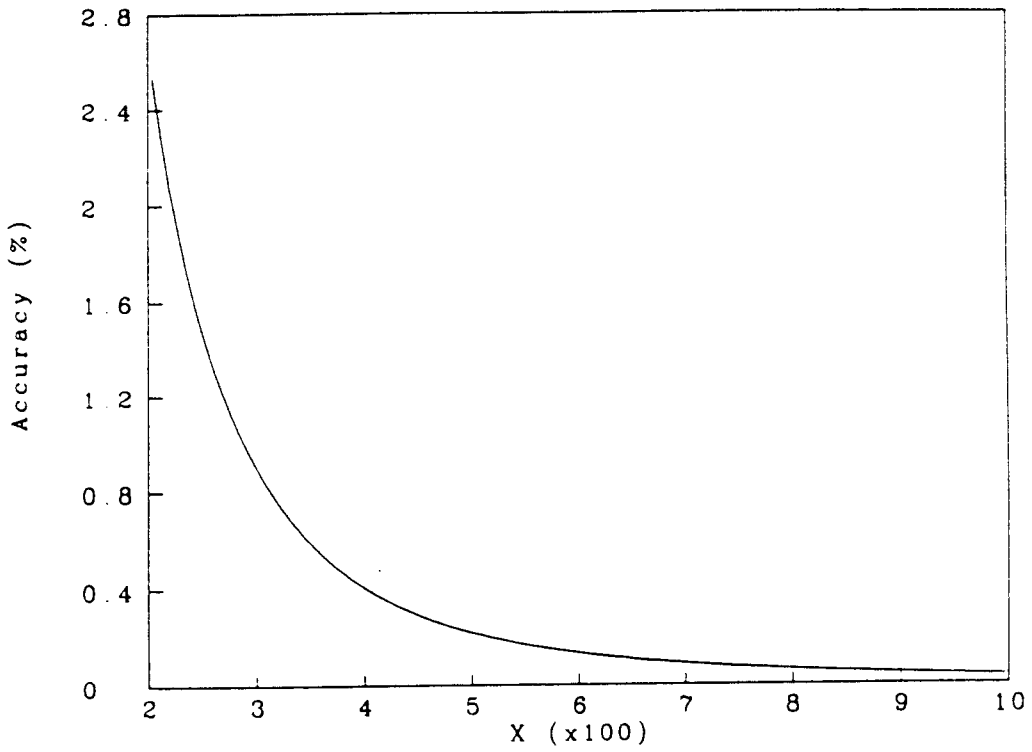

Figure 6. Relative accuracy of Grotch's approximate decay spectrum for use above $E_e > 3m_e$, relative to his exact first-order expression.

Appendix D

Monte Carlo Physics — TRIM

The stopping distribution of heavy particles for one special case—that of a fixed energy beam normally incident on a homogeneous, semi-infinite medium—is fairly well understood. However, analytic calculations are not generally applicable to real experiments; measurements find both shorter average ranges and asymmetric stopping distributions about the average because of large angle scattering. More complex geometries cause further complications.

Realistic stopping distributions can be obtained through Monte Carlo calculation. The TRIM85[1] code implements this for low-energy ions of hydrogen through uranium incident on a wide variety of materials. It must be noted, however, that the source code provided does not contain all of the features attributed to it; alternative versions were used to obtain some of the results shown in the book by Ziegler *et al.*

This code has been rewritten extensively, so as to apply it to the problem of a μ^+ stopping in a complex geometry. Geometrical, input and output routines are separated from the routines involved with physics, emulating the approach used in the EGS package. The physics in TRIM85 is improved as needed, including the insertion of intrinsic straggling and an iterative algorithm to find the energy loss during a step. The TRIM85 dE/dx values

[1] J. F. Ziegler, J. P. Biersack and U. Littmark, *The Stopping and Range of Ions in Solids* (Pergamon Press, New York, 1985) Vol. 1.

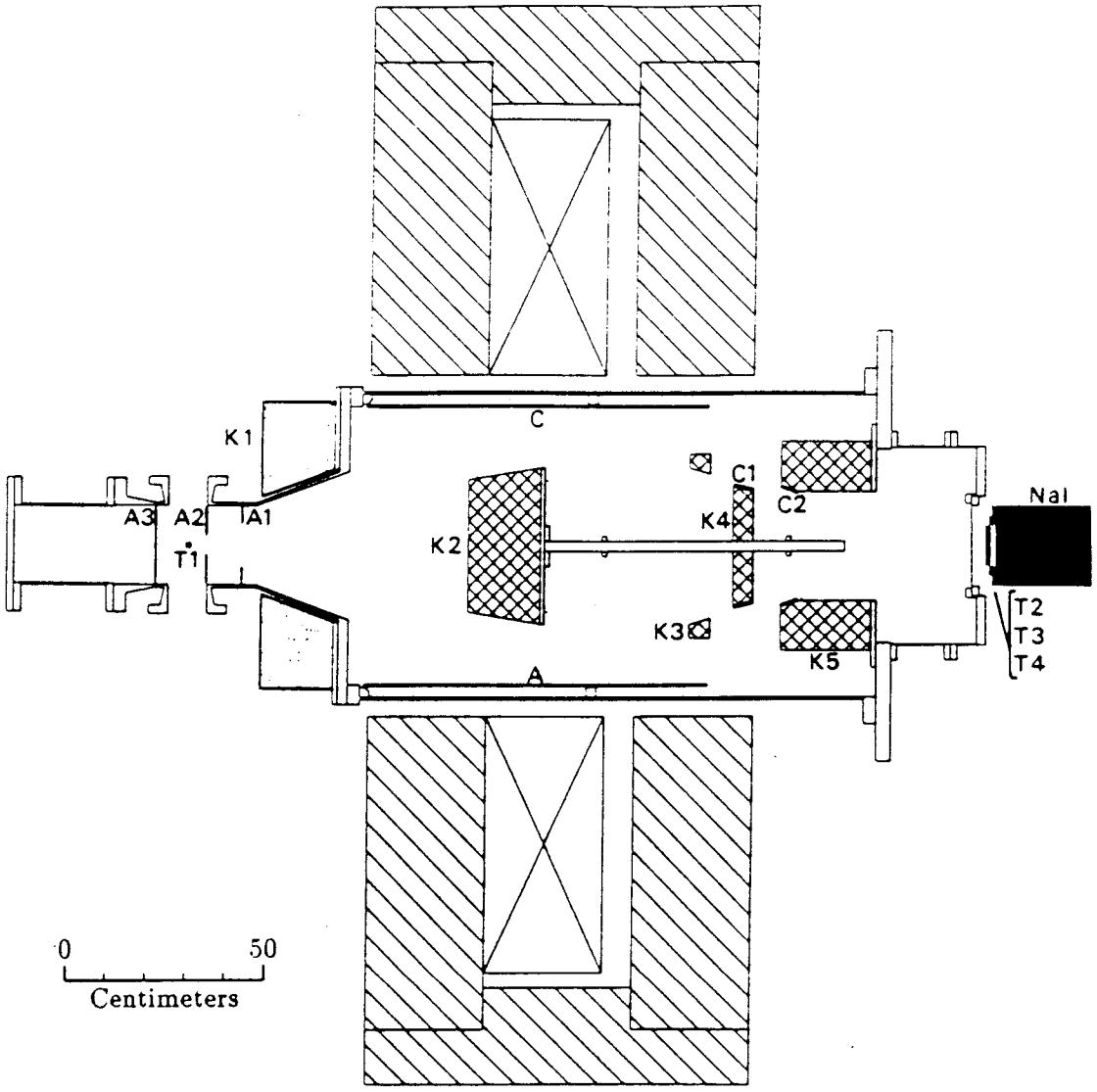

Figure 8. Vertical section through the Comus spectrometer. The dotted lines represent the collimator-support cables, projected onto this plane.

0.5%. Based on Bethe's quantitative comparison with the exact theory of Goudsmit and Saunderson,[22] it does not appear that multiple scattering uncertainties at small angles should be important when the step sizes in EGS are not large.

One shortcoming in the EGS treatment that must be noted is this: scattering from atomic electrons below the threshold for discrete treatment is included as a multiplicative correction to Molière scattering, approximating the electrons as, basically, protons. This is obviously incorrect for scattering at angles of more than 90°. For a discrete treatment limit of 89 KeV kinetic energy, such as was typically used in running EGS, the maximum pseudo-elastic single scattering angle of 6 MeV positrons from electrons should actually be 2.8°. For 50 MeV positrons, the angle becomes 0.35°. The approximation can be significant in light materials, such as NE110, where single scatters at large angles are overstated by 17%. Fortunately, backscattering has fairly low probability in light materials. The primary effect in this experiment was to reduce the calculated detection efficiency slightly; this was corrected by hand.

Calculations of backscattering from active media (such as the $T3$ counter) are biased by another effect which is inherent in a condensed history Monte Carlo such as EGS. Particles are propagated a finite distance before "continuous" effects like multiple scattering are considered. This means that energy deposition by a backscattered particle in a scintillator will be overstated, since it usually results from a single nuclear scatter that occurred before the end of the step. Reducing step sizes near the surface, as is done by PRESTA, reduces the bias (but does not eliminate it, since the step sizes are not reduced below some finite limit). In principle, it would be nearly possible to eliminate this problem by treating single scatters of more than some cutoff angle as a discrete process to be included in the reaction cross section.

In their evaluation of the accuracy of the treatment of backscattering by PRESTA, Bielajew and Rogers[23] found that the fraction of energy reflected from a semi-infinite slab showed

[22] S. A. Goudsmit and J. L. Saunderson, Phys. Rev. **57**, 24 and **58**, 36 (1940).

[23] Alex F. Bielajew and David W.O.Rogers, Report PIRS 042, pp.29-30, 1986.

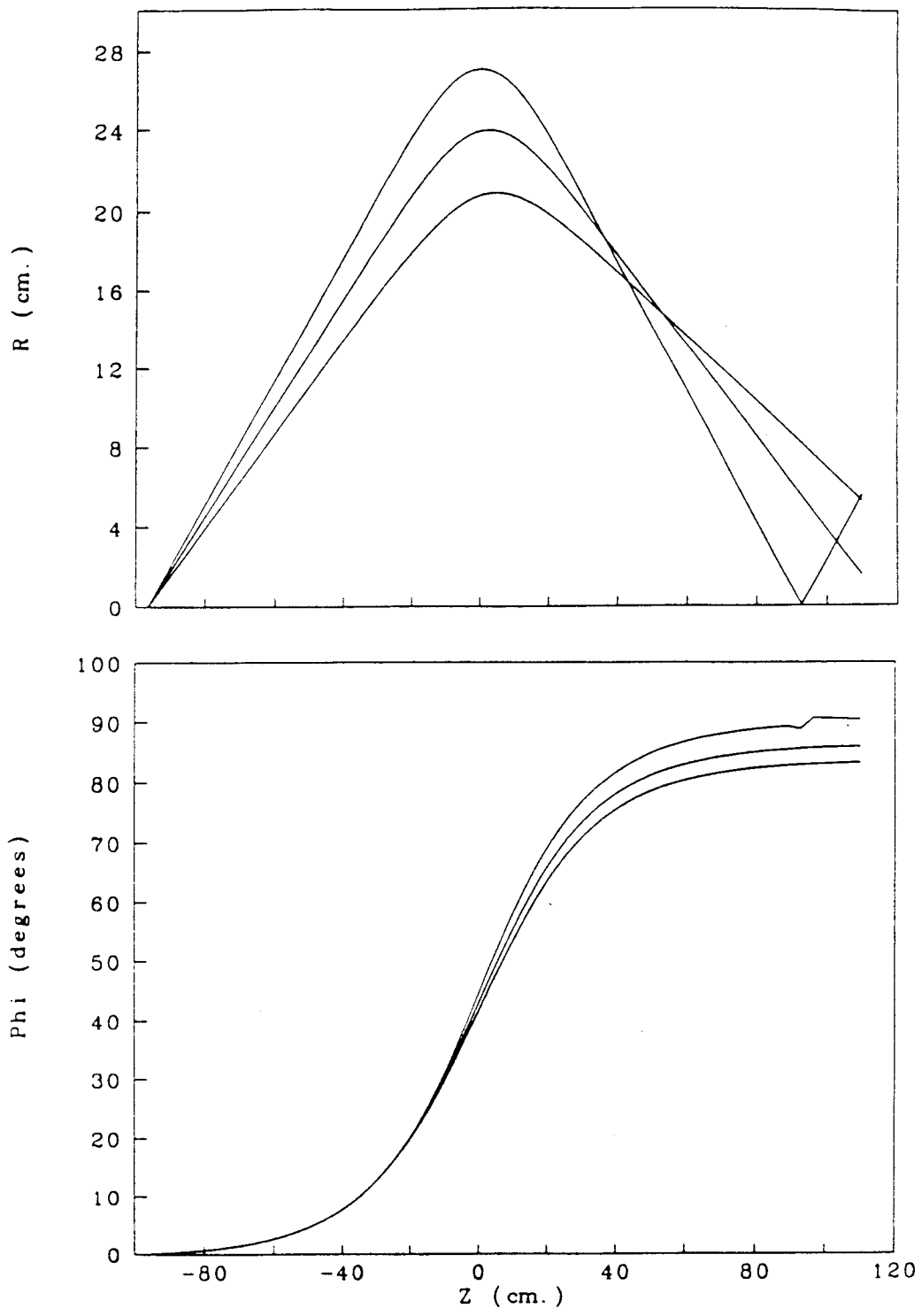

Figure 10. Typical accepted trajectories calculated for the Comus spectrometer. Note the approximate ring focus in the radial distribution.

C.6 Bhabha Scattering

The separate treatment of Bhabha scattering and bremsstrahlung in the field of an electron is fundamentally artificial, since Bhabha scattering is always accompanied by real photon emission (Bloch-Nordsieck argument) and electrons recoil from the passing of the virtual photon in bremsstrahlung. However, they are treated separately both in the literature and in EGS.

The radiative corrections can, in principle, have a large fractional effect on the cross section for Bhabha scattering. This is especially true for large energy transfers, since the energy carried off by real photons drives the cross section to zero.[12] Unfortunately, available calculations of the radiative corrections are not directly applicable to this experiment, having been done in the soft photon approximation,[13,14,15] for virtual photons only,[16] for ultra-relativistic energies,[17] for large energy transfers[18] or for specific experiments.

The Bhabha scatters of most importance to this experiment are those in which positrons of 20-53 MeV lose 10-50% of their energy to relatively low-energy electrons. The soft photon calculations predict reductions of a few percent, but have a photon energy cutoff in a logarithmic term and so do not give a definite prediction; plausible cutoffs yield reductions of 1-10%. The virtual photon calculations of Furlan and Peressutti predict a reduction of about 1% in the probability of Bhabha scatters for energy transfers of around 20%. The ultra-relativistic formula predicts a reduction of 5-6%, and, in the large energy transfer formula, the cross section is lowered by 10%. Thus, a reasonable estimate for the cross-section reduction is $(5 \pm 4)\%$.

---

[12] A. C. Hearn, P. K. Kuo and D. R. Yennie, Phys. Rev. **137**, 1950 (1969).

[13] A. I. Akhiezer and R. Polovin, Doklady Akad. Nauk USSR, **90**, 55 (1953).

[14] M. Redhead, Proc. Roy. Soc. (London) A **220**, 219 (1953).

[15] R. Polovin, JETP, **31**, 449 (1956), Sov. Phys. JETP, **4**, 385 (1957).

[16] G. Furlan and G. Peressutti, Nuovo Cimento **19**, 830 (1961).

[17] A. I. Akhiezer and V. B. Berestetskii, in *Quantum Electrodynamics* (Interscience Publishers, New York, 1965), p. 730.

[18] A. C. Hearn, P. K. Kuo and D. R. Yennie, Phys. Rev. **137**, 1950 (1969).

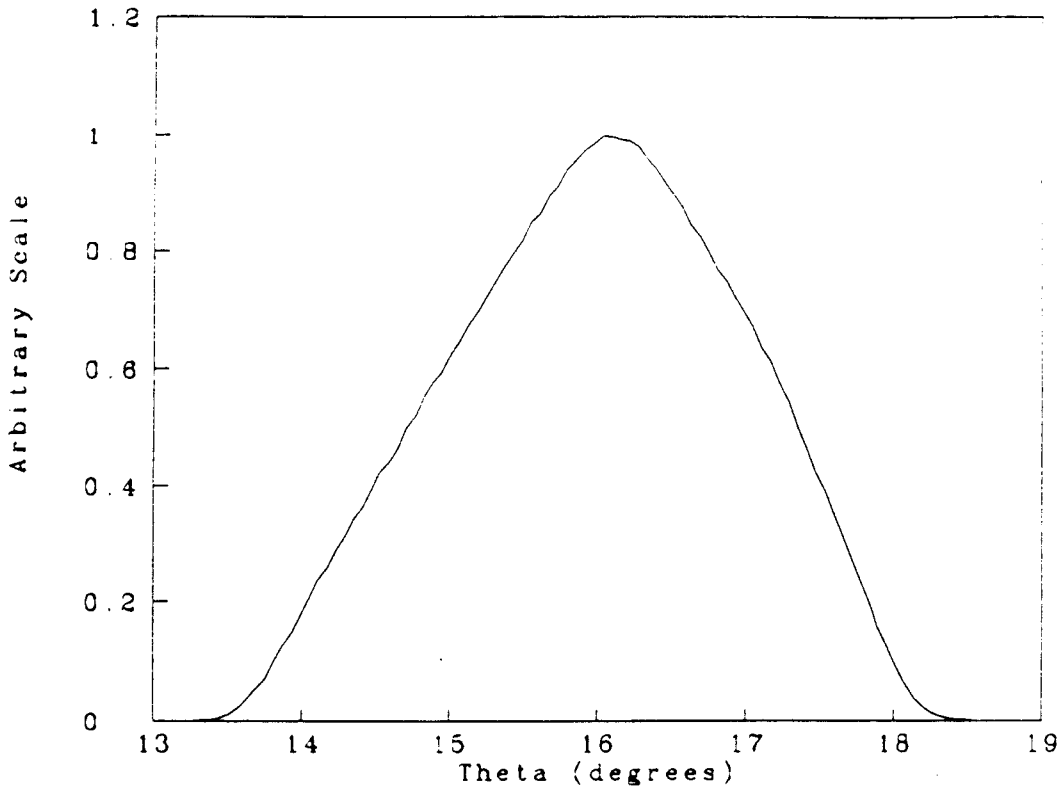

Figure 12. Calculated angular acceptance, averaged over momenta, of the Comus spectrometer at $T1$.

impact in this experiment; bremsstrahlung, though, is important.

While the relative inaccuracy is small for heavy elements (nuclear bremsstrahlung being larger by a factor of $O(Z)$), the distinction between the two processes can be important for materials containing only light elements. Plastic scintillator, in which carbon ($Z = 6$) is the heaviest component, is a potential problem. This is especially true for low-energy primaries, for which the electron to nuclear ratio is much less than the high-energy limit. Thus, EGS4 has been modified to treat bremsstrahlung in the field of electrons more accurately, using a table of cross sections found from numerical integrations of a formula derived by E. Haug[7], which is too lengthy to justify its inclusion here. Also incorporated were the suggestions of the ICRU[8] with regard to the treatment of the shielding problem and the formula's applicability to e^+ above energies of 5 MeV, since Haug's result is, strictly speaking, applicable only to the scattering of two free e^-.

In this way EGS4 was given the correct stopping power due to bremsstrahlung in the electron field, but this was still done with a multiplicative correction factor to avoid extensive changes in the code. This is to say that the differential cross section was still not correct. For NE 110, hard bremsstrahlung was overemphasized by about 4.5%, while very soft bremsstrahlung was too small by as much as 17%.

Another thing to consider is that bremsstrahlung processes are not given the correct angular distributions for the final particle directions in EGS. In fact the lepton is not assumed to change direction when emitting bremsstrahlung, and the photon is always taken to be emitted at the same polar angle with respect to the lepton. The justification for the former, as given by the authors of EGS, is that multiple scattering dominates over the deflection from bremsstrahlung. In materials thicker than about 0.0025 radiation lengths, this is true. Fortunately, the absolute values of the angles involved are small enough that there is no significant effect in this experiment even when this condition is not met. The use of the average for the photon angle also presents no problem: the angles involved are

[7] E. Haug, Z. Naturforsch **30a**, 1099 (1975).

[8] International Commission on Radiation Units and Measurements, Report 37 (1984).

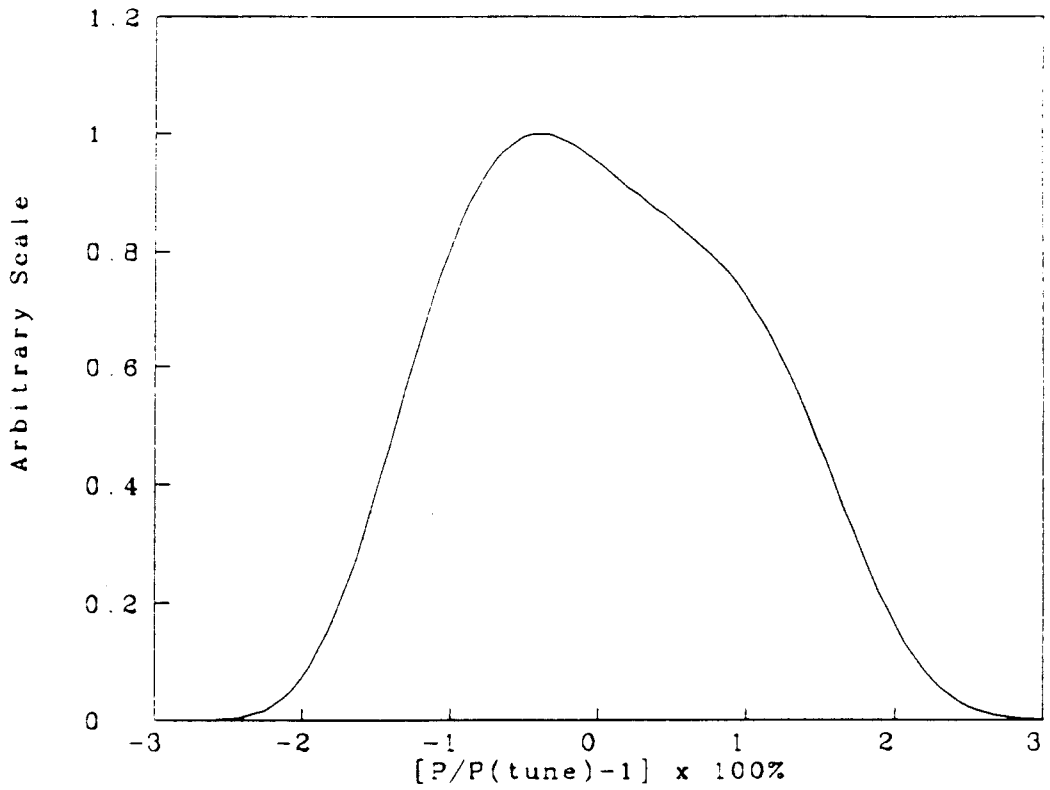

Figure 14. Calculated line shape of Comus spectrometer at $T1$. Note the break in the slope of the high momentum edge from the use of two separate collimators ($K3$ and $C2$).

in the Monte Carlo simulation until after the first path length has been traversed, the scattering may not be relevant any more—enough energy may have already been deposited in the calculation to produce an event "veto".

- If a charged particle is travelling close to, and nearly parallel to, a material boundary, the calculated results can depend strongly upon the path-length limit. The reason, of course, is that a tiny scattering may allow the particle to escape from the region in a much shorter distance than would be needed if a straight path were followed. One place where this problem arises is in the scattering of grazing incidence particles from collimators. Another is in the muon-stopping target, $T1$, which is very thin compared to its height and width; some of the e^+ will be produced with initial trajectories nearly in the target plane, but can occasionally scatter into the spectrometer acceptance. EGS will naively move particles a distance of a centimeter or more before considering the possibility of a scatter, while the real particles will often scatter out of the target well before that distance and, thus, be scattered at smaller angles than found by EGS. For these reasons, EGS may give erroneous values for both the energy deposition in the target and the likelihood of a particle scattering into the spectrometer acceptance, unless one stringently limits the allowable path length per step.

A package of macros referred to as PRESTA[6] is available to improve the particle transport in EGS4. In addition to including a boundary crossing and lateral transport algorithm, so that the above problems are more accurately handled, it handles the multiple scattering path-length correction in a way that is consistent with the multiple scattering treatment. This means that results are nearly independent of step size—which is not always the case with uncorrected EGS4 at low energy.

Most of the programs used to simulate the Comus spectrometer incorporated PRESTA. This macro package was generalized to allow region-by-region adjustment of the algorithm, increasing the speed and/or accuracy in most applications.

[6] Alex F. Bielajew and David W.O.Rogers, Report PIRS 042, 1986.

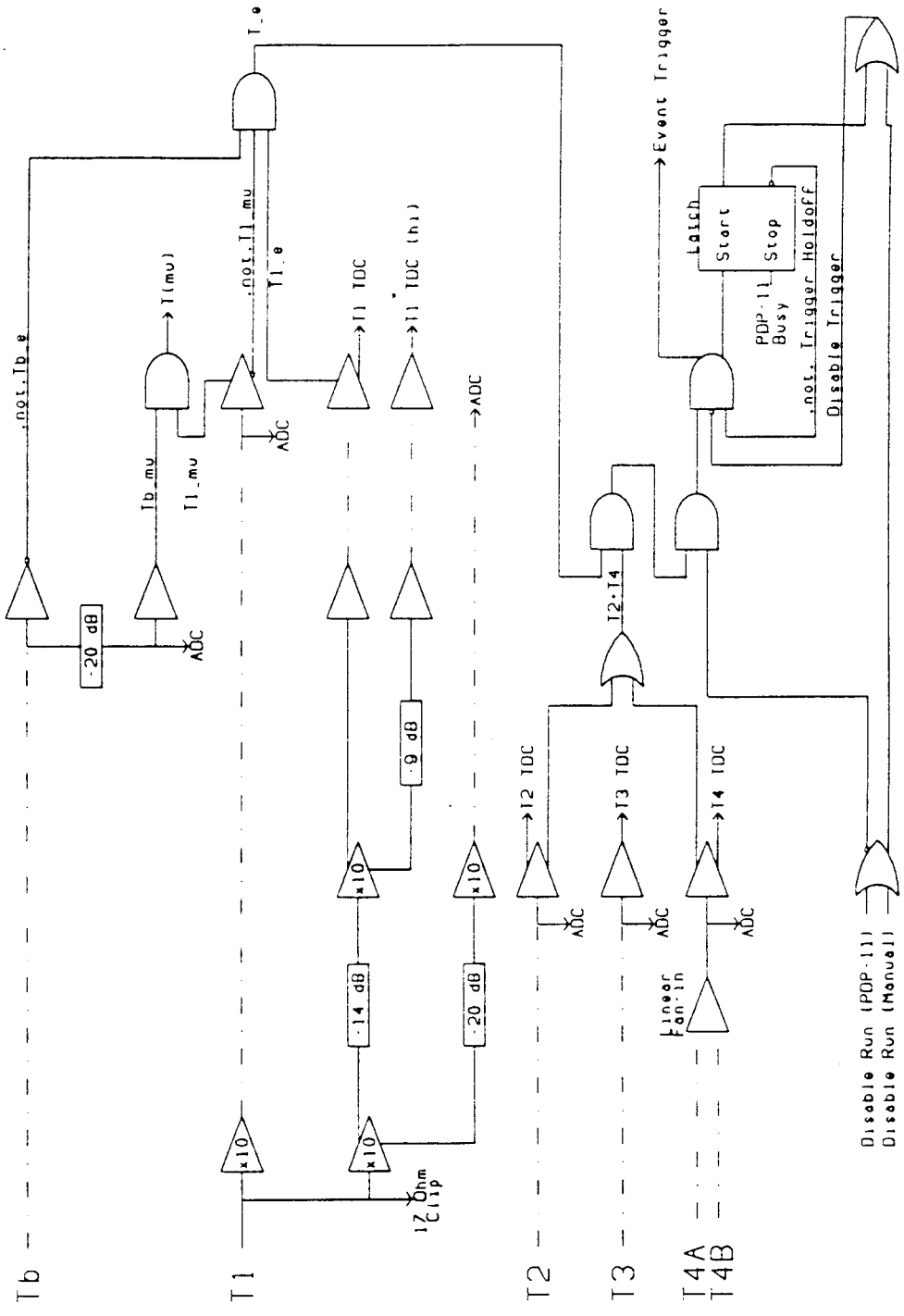

Figure 16. The trigger electronics, slightly simplified. Unlabled triangles represent discriminators. The electronics to the left of the dot/dash lines were in the experimental area, with the remainder in the counting room.

a counter, though there are also many examples among the physical processes which the particles undergo.

In such a situation, one would like to propagate a particle over a fairly long step and choose the energy loss from a known distribution depending on the incident particle's characteristics, the material and step size. This is easily implemented: EGS provides the average energy loss and one need only randomly choose a value from the energy-loss distribution whose average is equal to this. The particular one chosen was the Blunke-Leisegang distribution, which is somewhat broader and more accurate than the Landau distribution for thin lamina, becoming very similar for thick lamina. It is composed from the sum of four Gaussian curves whose relative weights, widths and centroids were chosen from empirical data. In order to choose a properly weighted variable from this distribution, one need only choose which of the four Gaussians to use, based on their relative weights, and then randomly sample from a Gaussian of this width and centroid.

There are, in general, problems of internal consistency with this approach, appearing in some dependence of the energy-straggling width on the step sizes taken to travel a given distance. This arises from the fact that the tails of distributions like that of Landau or Blunke-Leisegang do not join smoothly with the discrete energy-loss distribution; the tails are not of the correct shape and include energy losses past the threshold for discrete production. The distributions are accurate only in the region around the average energy-loss peak. Nonetheless, straggling can be incorporated in this way with reasonable accuracy, provided that the step size is small enough that the tail of the continuous loss distribution does not extend significantly past the discrete treatment threshold and that a trajectory through a region is not heavily subdivided. Also, errors are usually partially corrected by folding the energy-loss distribution with a resolution curve to reproduce the measured width of the ADC of a counter.

Another potential problem is the choice of the threshold for discrete production. If this threshold is too low, the calculation becomes hopelessly time-consuming, while, if too high, the real particles may escape from a thin lamina (such as $T1$) and cause effects (such

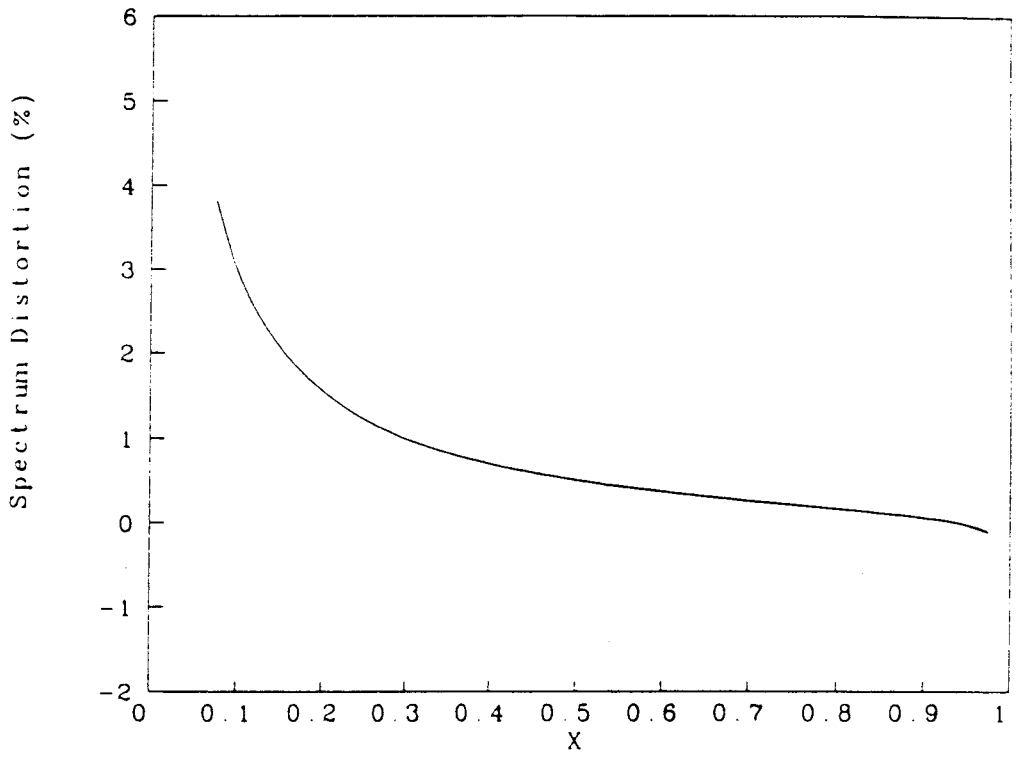

Figure 18. Relative effect on the spectrum of continuous energy losses in $T1$.

Appendix C

Monte Carlo Physics — EGS

C.1 Introduction to EGS

The EGS4 Code System[1] is a general purpose program for the simulation of electromagnetic showers. It extends the capabilities of, and corrects errors in, EGS3.[2] This latter code was used in the earlier part of the analysis of this experiment, until EGS4 was released and could be implemented. The total dynamic kinetic energy range is claimed to be from a few tens of KeV to a few thousand GeV for charged particles and from 1 keV to a few thousand GeV for photons. This covers the energy range with which a muon decay experiment is likely to concern itself. The relevant physics are largely contained within this code system, with the user being mostly required to initialize the particle characteristics and trajectories, to handle of the geometry for particle propagation and to extract information from the particle showers. For high-quality results, the user must also carefully choose various parameters (such as thresholds for discrete particle treatment), balancing CPU time requirements against accuracy.

Given the historical development of EGS for medical physics and high-energy calorimetry, it is not surprising that time is not handled in the program at all. This means, barring

[1] W. R. Nelson, H. Hirayama and D. W. O. Rogers, SLAC **265** (1985).

[2] R. L. Ford and W. R. Nelson, SLAC **210** (1978).

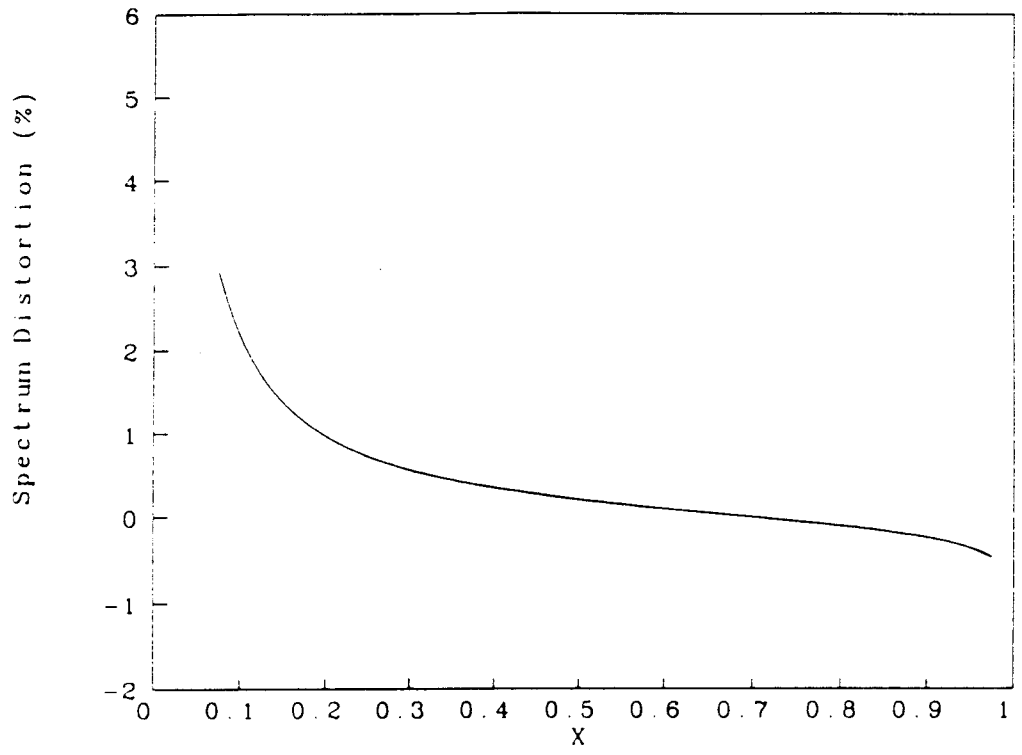

Figure 20. Relative effect on the spectrum of external bremsstrahlung in $T1$.

size. Since the surface area available for passive cooling scales as b^2, while the heat produced for a given gradient compensation scales as, at least, b^4, this is clearly desirable.

B.2.2 Canceling $\frac{\partial B_z}{\partial y}$

The procedure for canceling this gradient is similar. Again, the field is found at $(0,0)$ from four filaments placed at $(\pm a, \pm b)$, except that they now all carry a current I in the -$\hat{x}$ direction. B_z and all its even derivatives with respect to y vanish, while

$$\frac{\partial B_z}{\partial y} = \frac{2}{b^2}\frac{\mu_0 I}{\pi}\frac{q^2-1}{(1+q^2)^2} \qquad \text{and} \qquad \frac{\partial^3 B_z}{\partial y^3} = \frac{12}{b^4}\frac{\mu_0 I}{\pi}\frac{1-6q^2+q^4}{(1+q^2)^4}\,.$$

Much as before, the higher derivatives can be ignored and several values of q can be chosen which, taken together, minimize $\partial^3 B_z/\partial z^3$ and maximize $\partial B_z/\partial z$. Again, one should try to minimize b.

B.3 Other Considerations

When the absolute size of the gradients to be compensated is large, substantial current densities are required in the compensating coils. As an example, when Comus was tuned to the muon decay endpoint, $\partial B_z/\partial y = 220$ gauss/cm. About 60 amps were required to cancel this gradient in the coils built for this experiment. While the absolute size of the current stems from the use of only four sets of conductors (which maximized the conductor filling factor and simplified the conductor positioning), the current density would be high for any design and implies substantial heating. It is for this reason that printed circuit techniques[2] were rejected in favor of a machined coil form and #14 copper wire. Even then, forced air cooling was required.

[2]The printed circuit compensating coils discussed by K. Borer and G. Fremont for use with the CERN NMR probes were rated at 20 gauss/cm; these probes are substantially thinner than the LBL-designed probes and compensation therefore requires less current.

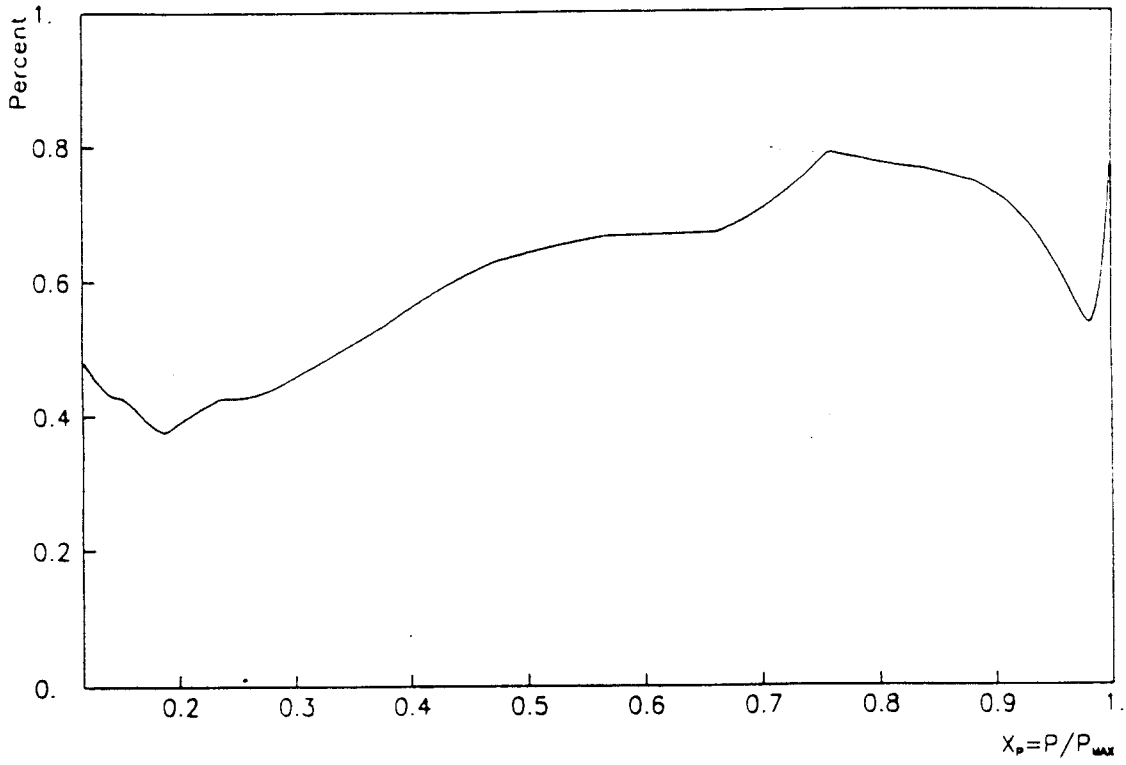

Figure 22. Relative spectrum effect due to the three upstream sets of collimator-suspension cables, as calculated by Monte Carlo. The reduced effect above $x_p = 0.75$ is due to the absence of particles incident on the cables from above the spectrum endpoint, while the rise near $x_p = 1$ is due to the drop in the number of normal events near the endpoint.

are four conditions imposed on the field derivatives by Maxwell's equations:

$$\vec{\nabla} \cdot \vec{B} = 0$$

$$\vec{\nabla} \times \vec{B} = 0 \, .$$

The remaining derivatives to eliminate at the probe center are

$$\frac{\partial B_x}{\partial x} = \frac{\partial B_x}{\partial y} = \frac{\partial B_x}{\partial z} = \frac{\partial B_z}{\partial y} = \frac{\partial B_z}{\partial z} = 0 \, .$$

Several of these conditions could be achieved through the symmetries of the magnet. With right-handed Cartesian coordinates $\hat{x}$,$\hat{y}$,$\hat{z}$, whose origin is not on the magnet's axis, $\hat{x}$ is defined to be tangential to a circle around the symmetry axis, $\hat{y}$ to be radially inward and $\hat{z}$ to be parallel to the symmetry axis. Then, because Comus is axially symmetric with no significant azimuthal field components, $B_x = 0$ at $x = 0$ and, therefore,

$$\frac{\partial B_x}{\partial y} = \frac{\partial B_x}{\partial z} = 0 \, .$$

One more condition can be satisfied by appropriately choosing the value of z at which the probe is placed. If B_r is the radial field component at a distance r from the symmetry axis, then

$$\frac{\partial B_x}{\partial x} = \frac{B_r}{r} \, .$$

Thus, this derivative vanishes where $B_r = 0$, which will be true for some z near the spectrometer midplane at any radius—for a spectrometer which is nearly symmetric across this midplane.

Alternatively, one could choose a value of z at which there was an extremum in B_z, thereby eliminating $\partial B_z/\partial z$. Both this and the $B_r = 0$ condition would be fulfilled at a single point if the magnet were completely symmetric across the midplane, but this was not quite true for Comus. Forced to choose which of the two conditions to satisfy, one should note that it is much easier to act upon two derivatives of the same field component for engineering reasons. Thus, z was chosen such that

$$\frac{\partial B_x}{\partial x} = 0$$

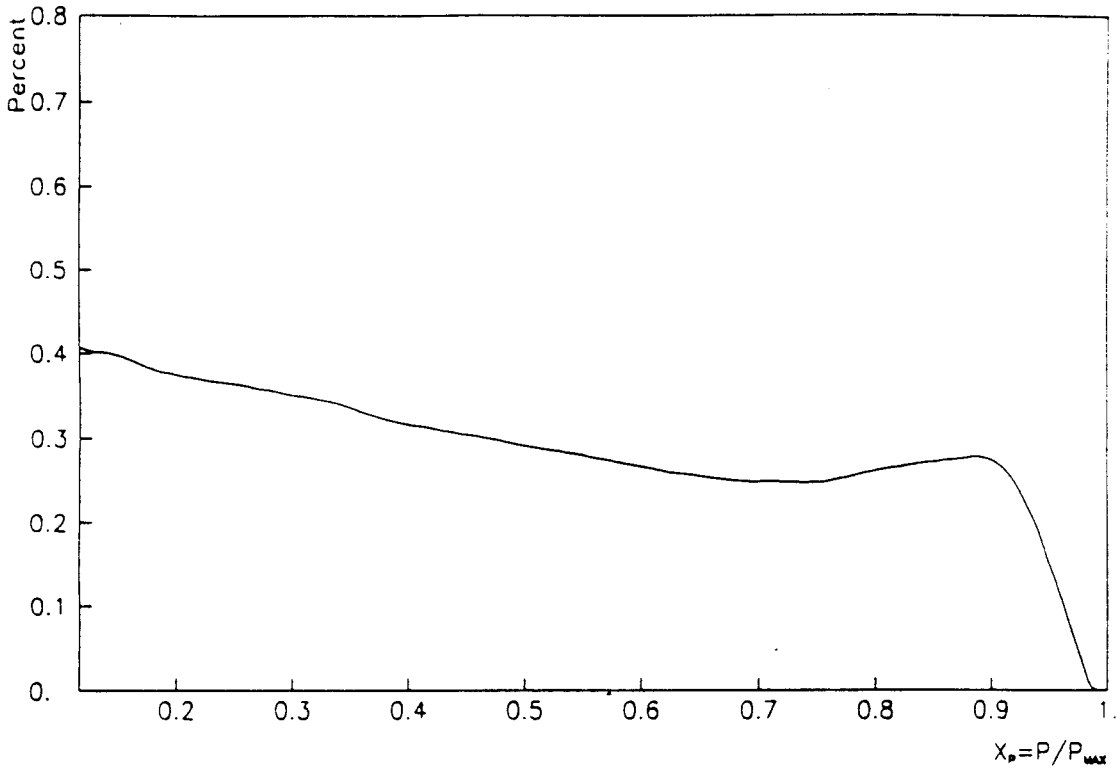

Figure 24. Relative spectrum effect of scatters from the bevel of the $K3$ collimator, as calculated by Monte Carlo. The drop for $x_p > 0.9$ is due to the absence of incident particles from above the endpoint momentum.

such as the aforementioned light guide on $C1$ would not be much of a problem anyway: the fractional spectrum distortion at $x = 0.1$ is only a negligible 0.005% for a muon polarization of 0.25. In fact, any reasonable effort to produce an azimuthally uniform acceptance would avoid problems in this particular experiment.

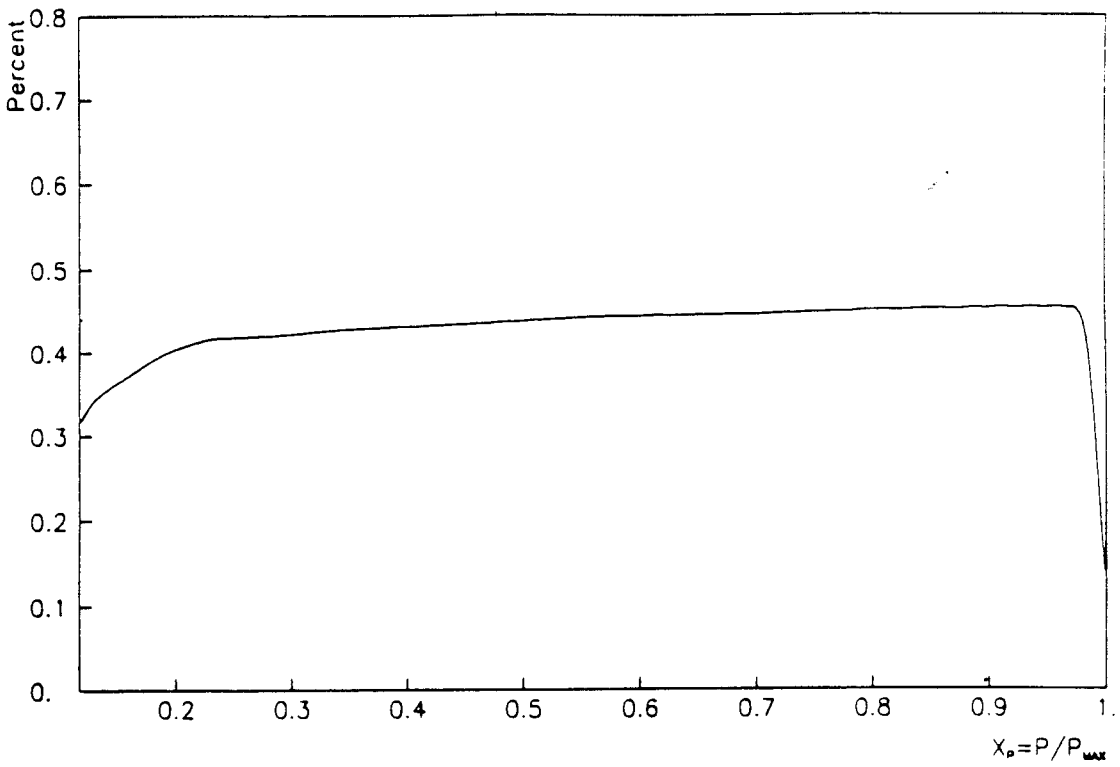

Figure 26. Relative spectrum effect of scatters from $C2$, as calculated by Monte Carlo. The dip near $x_p = 1$ arises from the number of particles on $C2$ falling off more rapidly than the number accepted, since $C2$ forms part of the high side of the momentum selection slit.

This result can be used to find, for example, the spectrum distortion that could result from the target not being centered in the magnetic field of Comus. From field measurements,

$$\sin\theta_B = (0.0244\,\mathrm{cm}^{-1})r$$

at the target position for small radial displacements, r. Applying this measurement to the above results,

$$\frac{\Delta\mathcal{P}(x)}{\mathcal{P}(x)} < \alpha(x)\frac{0.0244}{\mathrm{cm}}r\ .$$

A.2 Misaligned Muon Spin

Consider now another possibility—that the muon spin is not quite along the $\hat{x}$ direction as assumed, but is at an angle ϵ from the $\hat{x}$-$\hat{y}$ plane. This might, for example, arise from misalignment of the spectrometer with respect to the beam line. (Deviations which are not out of that plane make no difference.) It will be assumed that no other asymmetries exist: that the spectrometer acceptance is azimuthally symmetric and the magnetic field at the target is uniform and along $\hat{z}$. In the same notation as Section A.1,

$$\hat{\mu}(t) = \hat{x}\cos\omega t\cos\epsilon + \hat{y}\sin\omega t\cos\epsilon + \hat{z}\sin\epsilon\ .$$

Then the angle between the muon spin and an accepted positron is given by

$$\cos\gamma(t) \equiv \hat{\mu}(t)\cdot\hat{e} = \sin\theta_a\cos\epsilon\,(\cos\phi_a\cos\omega t + \sin\phi_a\sin\omega t) + \cos\theta_a\sin\epsilon\ ,$$

which leads us to the equation

$$\begin{aligned}\mathcal{P}(x) &\propto \int_0^\infty \tfrac{dt}{\tau}\exp(-\tfrac{t}{\tau})\int_{\theta_1}^{\theta_2}\sin\theta_a d\theta_a\int_0^{2\pi}[1+\alpha(x)\cos\gamma(t)]\,d\phi_a \\ &\propto A\,[1+\alpha(x)<\cos\theta_a>\sin\epsilon]\ .\end{aligned}$$

There is, of course, no dependence upon ω in this equation since the angle between the muon spin and the spectrometer acceptance is constant; any distortion of the spectrum would arise from the energy-dependence of $\alpha(x)$. For the Comus spectrometer, again using $<\cos\theta_a>\approx 1$, the upper limit on the fractional error is then obtained as

$$\frac{\Delta\mathcal{P}(x)}{\mathcal{P}(x)} \leq \alpha(x)\sin\epsilon\ .$$

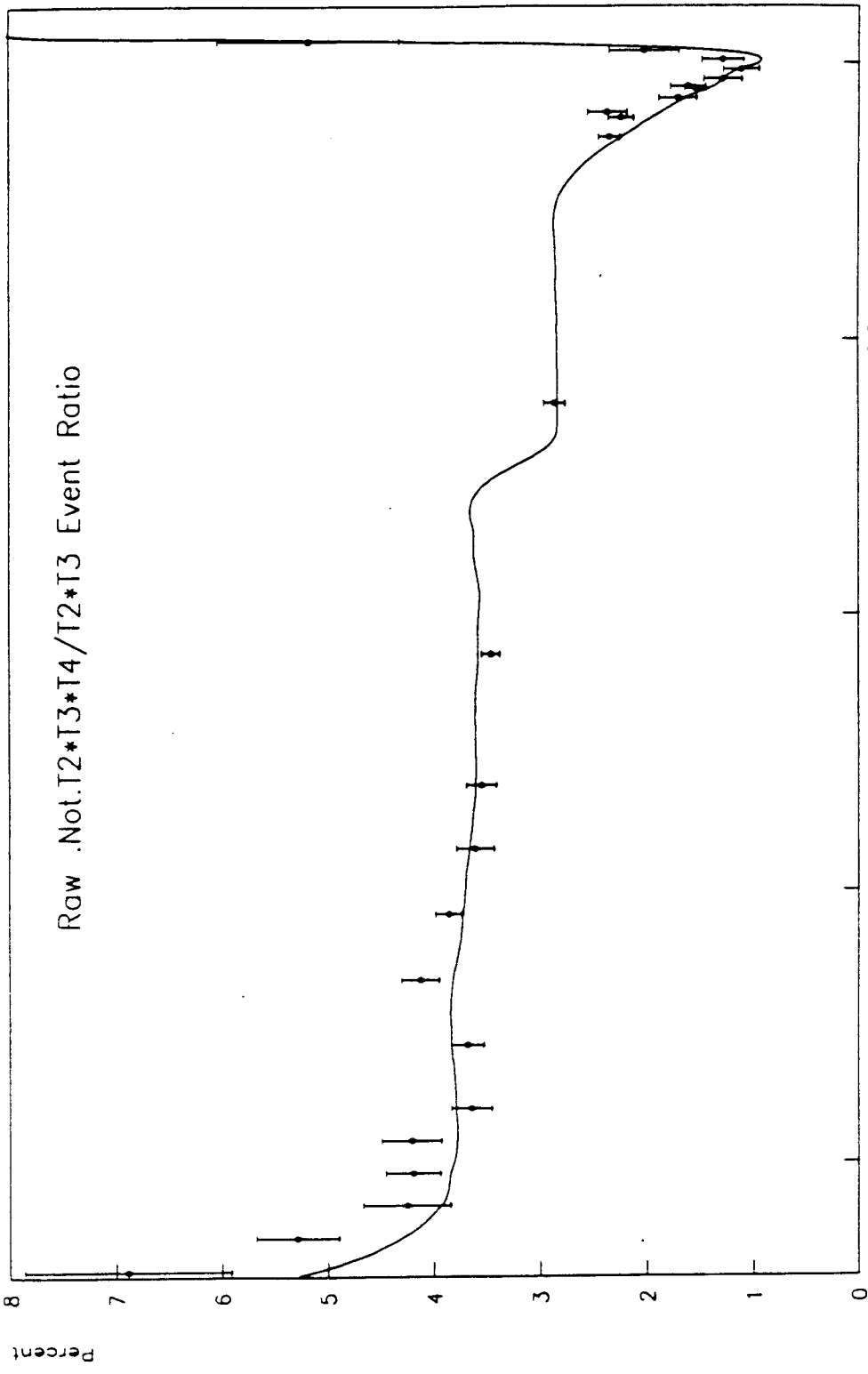

Figure 28. Comparison of the measured and calculated $T2 \cdot T3/\overline{T2} \cdot T3 \cdot T4$ ratio. The calculation is from first principles; the measured points are shown with only the statistical errors of the data.

- The incoming beam pipe is surrounded by magnetic shielding near the target which might, in principle, distort the field there.
- The earth's field is certainly not along the spectrometer axis and, at low P_{tune} would cause a significant problem if the flux lines were not adequately shunted away by the nearby iron.

A second system of coordinates $\hat{x}'$,$\hat{y}'$,$\hat{z}'$ and angles θ_B,ϕ_B are now defined. The direction of $\hat{z}'$ is defined to be along $\vec{B}$ at the muon position, separated from $\hat{z}$ by the angle θ_B. The coordinate transformation is given by

$$\begin{aligned}
\hat{x}' &= \hat{x}\cos\theta_B\cos\phi_B + \hat{y}\cos\theta_B\sin\phi_B - \hat{z}\sin\theta_B \\
\hat{y}' &= -\hat{x}\sin\phi_B + \hat{y}\cos\phi_B \\
\hat{z}' &= \hat{x}\sin\theta_B\cos\phi_B + \hat{y}\sin\theta_B\sin\phi_B + \hat{z}\cos\theta_B \ .
\end{aligned}$$

If $\hat{\mu}(0)$ is the unit vector along the initial spin direction of the muon

$$\hat{\mu}(0) = \hat{x} = \hat{x}'\cos\theta_B\cos\phi_B - \hat{y}'\sin\phi_B + \hat{z}'\sin\theta_B\cos\phi_B \ .$$

At later times, $\hat{\mu}$ will precess around $\hat{z}'$ with angular frequency ω:

$$\begin{aligned}
\hat{\mu}(t) = \ & \hat{x}'(\cos\omega t\cos\theta_B\cos\phi_B + \sin\omega t\sin\phi_B) + \\
& \hat{y}'(\sin\omega t\cos\theta_B\cos\phi_B - \cos\omega t\sin\phi_B) + \\
& \hat{z}'\sin\theta_B\cos\phi_B \ .
\end{aligned}$$

In spectrometer coordinates this would be

$$\begin{aligned}
\hat{\mu}(t) = \ & \hat{x}\left[\cos\omega t + \sin^2\theta_B\cos^2\phi_B(1-\cos\omega t)\right] + \\
& \hat{y}\left[(1-\cos\omega t)\sin^2\theta_B\cos\phi_B\sin\phi_B + \sin\omega t\cos\theta_B\right] + \\
& \hat{z}\sin\theta_B\left[(1-\cos\omega t)\cos\theta_B\cos\phi_B - \sin\omega t\sin\phi_B)\right] \ .
\end{aligned}$$

Consider now a decay positron whose polar and azimuthal angles in the spectrometer, θ_a and ϕ_a, are such as to allow acceptance. The positron's unit direction vector is then given by

$$\hat{e} = \hat{x}\sin\theta_a\cos\phi_a + \hat{y}\sin\theta_a\sin\phi_a + \hat{z}\cos\theta_a \ .$$

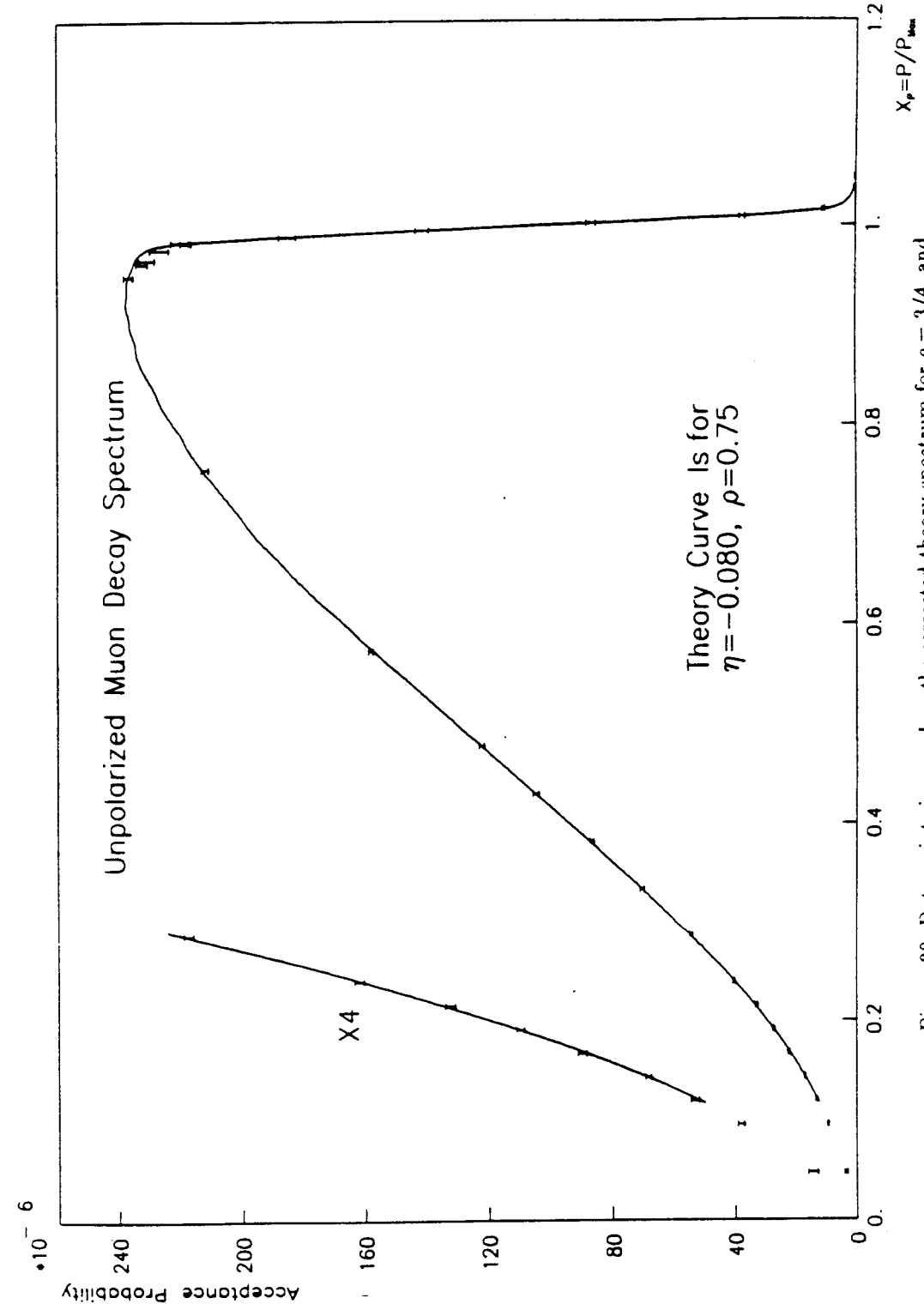

Figure 30. Data points imposed on the corrected theory spectrum for $\rho = 3/4$, and the best-fit values of η and amplitude normalization. Error bars represent only the statistical errors of the data.

Source	Geometry	References for Effect
μ^+ depth	Fig. 15, Sec. 4.1.5	Sec. 6.1.1, E.2.1
Back plate	Fig. 8	Fig. 27, Sec. 5.10, 6.6, E.2.2
$T1$	Fig. 15, Sec. 4.1.5	Fig. 17-20, Sec. 5.1, 6.1.2, E.2.3
Detector ineff.	Fig. 8, 11, Sec. 4.1.8	Fig. 21, Sec. 5.2, 6.1.6, E.2.4
μ^+ spin angle		Sec. A.2, E.2.5
Cables	Fig. 8	Fig. 22, Sec. 5.3, 6.1.5, E.2.6
$K2$	Fig. 8, Sec. 4.1.6	Fig. 23, Sec. 5.5, 6.1.4, E.2.7
$C1$	Fig. 8, Sec. 4.1.6	Fig. 25, Sec. 5.9, 6.1.4, E.2.8
P_{max} calib.	Sec. 4.1.1	Sec. 6.4, B.4, E.2.9, 4.1.2
Beam centering		Sec. A.1, E.2.10
Muon stops	Fig. 15, 16	Sec. 6.5, E.2.11
$K3$	Fig. 8, Sec. 4.1.6	Fig. 24, Sec. 5.6, 6.1.4, E.2.12
Line shape	Fig. 13, 14, 30	Sec. E.2.13
$C2$	Fig. 8, Sec. 4.1.6	Fig. 26, Sec. 5.9, 6.1.4, E.2.14
Asymmetry		Sec. A.3, E.2.15
Miscellaneous	Fig. 8	Sec. 5.4, 5.7, 6.1.4, E.2.16

Table 6.2: References to information on the systematic errors.